PCT WORLD INTELLECTUAL PROPERTY ORGANIZATION
International Bureau

INTERNATIONAL APPLICATION PUBLISHED UNDER THE PATENT COOPERATION TREATY (PCT)

(51) International Patent Classification 6 : G06K 9/00, 9/40

A1

(11) International Publication Number: **WO 97/09690**

(43) International Publication Date: 13 March 1997 (13.03.97)

(21) International Application Number: PCT/US96/14500

(22) International Filing Date: 5 September 1996 (05.09.96)

(30) Priority Data:
08/523,438 5 September 1995 (05.09.95) US

(71) Applicant: NORTHROP GRUMMAN CORPORATION [US/US]; 1840 Century Park East, Los Angeles, CA 90067-2199 (US).

(72) Inventor: KRASKE, Wolfgang, Frederick; 16506 Windsor Avenue, Whittier, CA 90603 (US).

(74) Agents: ANDERSON, Terry, J.; Northrop Grumman Corporation, 1840 Century Park East, Los Angeles, CA 90067-2199 (US) et al.

(81) Designated States: AL, AM, AT, AU, AZ, BB, BG, BR, BY, CA, CH, CN, CZ, DE, DK, EE, ES, FI, GB, GE, HU, IL, IS, JP, KE, KG, KP, KR, KZ, LK, LR, LS, LT, LU, LV, MD, MG, MK, MN, MW, MX, NO, NZ, PL, PT, RO, RU, SD, SE, SG, SI, SK, TJ, TM, TR, TT, UA, UG, UZ, VN, ARIPO patent (KE, LS, MW, SD, SZ, UG), Eurasian patent (AM, AZ, BY, KG, KZ, MD, RU, TJ, TM), European patent (AT, BE, CH, DE, DK, ES, FI, FR, GB, GR, IE, IT, LU, MC, NL, PT, SE), OAPI patent (BF, BJ, CF, CG, CI, CM, GA, GN, ML, MR, NE, SN, TD, TG).

Published
With international search report.

(54) Title: DATA DIMENSIONAL SIEVING AND FUZZY CONNECTIVITY FOR MRI IMAGE ANALYSIS

(57) Abstract

In a method for isolating anatomical structures contained within a three-dimensional data set, a morphological skeleton (302) is first formed from the three-dimensional data set. Next, a seed data point (310) is selected from within the morphological skeleton. The seed data point is contained within a desired anatomical structure to be displayed and/or analyzed. Fuzzy connectivity (314) is utilized to define additional data points of the desired anatomical structure, so as to facilitate reconstruction of substantially only the desired anatomical structure. Such reconstruction of substantially only the desired anatomical structure facilitates viewing and analysis thereof by reducing complexity of the image and eliminating obstructing tissue.

FOR THE PURPOSES OF INFORMATION ONLY

Codes used to identify States party to the PCT on the front pages of pamphlets publishing international applications under the PCT.

AM	Armenia	**GB**	United Kingdom	**MW**	Malawi
AT	Austria	**GE**	Georgia	**MX**	Mexico
AU	Australia	**GN**	Guinea	**NE**	Niger
BB	Barbados	**GR**	Greece	**NL**	Netherlands
BE	Belgium	**HU**	Hungary	**NO**	Norway
BF	Burkina Faso	**IE**	Ireland	**NZ**	New Zealand
BG	Bulgaria	**IT**	Italy	**PL**	Poland
BJ	Benin	**JP**	Japan	**PT**	Portugal
BR	Brazil	**KE**	Kenya	**RO**	Romania
BY	Belarus	**KG**	Kyrgystan	**RU**	Russian Federation
CA	Canada	**KP**	Democratic People's Republic of Korea	**SD**	Sudan
CF	Central African Republic			**SE**	Sweden
CG	Congo	**KR**	Republic of Korea	**SG**	Singapore
CH	Switzerland	**KZ**	Kazakhstan	**SI**	Slovenia
CI	Côte d'Ivoire	**LI**	Liechtenstein	**SK**	Slovakia
CM	Cameroon	**LK**	Sri Lanka	**SN**	Senegal
CN	China	**LR**	Liberia	**SZ**	Swaziland
CS	Czechoslovakia	**LT**	Lithuania	**TD**	Chad
CZ	Czech Republic	**LU**	Luxembourg	**TG**	Togo
DE	Germany	**LV**	Latvia	**TJ**	Tajikistan
DK	Denmark	**MC**	Monaco	**TT**	Trinidad and Tobago
EE	Estonia	**MD**	Republic of Moldova	**UA**	Ukraine
ES	Spain	**MG**	Madagascar	**UG**	Uganda
FI	Finland	**ML**	Mali	**US**	United States of America
FR	France	**MN**	Mongolia	**UZ**	Uzbekistan
GA	Gabon	**MR**	Mauritania	**VN**	Viet Nam

DATA DIMENSIONAL SIEVING AND FUZZY CONNECTIVITY FOR MRI IMAGE ANALYSIS

Field of the Invention

The present invention relates generally to medical imaging systems and digital signal processing. It relates more particularly to the use of data dimensional sieving and fuzzy connectivity to facilitate analysis and review of three-dimensional medical images such as those produced by magnetic resonance imaging (MRI) devices and the like.

Background of the Invention

Tomographic imaging techniques for use in medical applications are well known. Examples of such techniques include magnetic resonance imaging (MRI), computer aided tomography (CAT), and positron emission tomography (PET). In each of these techniques, a plurality of cross-sectional two-dimensional images, i.e., slices, of a body portion are generated and processed so as to provide a three-dimensional model of the imaged body portion.

To utilize such a three-dimensional model of a body portion, slices or images taken along planes of interest are generated and then images are printed or otherwise displayed for viewing. The slices viewed may be at various angles with respect to the three-dimensional model. They do not necessarily correspond to the angles of the slides from which the three-dimensional model was originally constructed. Thus, the medical diagnostition may review images taken along any desired plane within the three-dimensional model. This provides for a great deal of flexibility in the use of the three-dimensional model as a

diagnostic tool.

As those skilled in the art will appreciate, such three-dimensional images provide a valuable tool to the medical diagnostition in a manner which is non-invasive, and which is therefore considered to be of very low risk to the patient.

However, although such three-dimensional imaging techniques have proven extremely useful for their intended purposes, they still possess inherent deficiencies which detract from their overall effectiveness. More particularly, it is frequently difficult to interpret the viewed two-dimensional slices or images when the anatomical structures of interest are surrounded by and/or intermixed with various other anatomical structures. The undesirable presence of such superfluous imagery only complicates the image, making it much more difficult to view and interpret the desired imagery.

For example, viewing delicate portions of the vascular system is typically difficult since veins, arteries, and capillaries are intermixed with surrounding tissue. This makes it very difficult to distinguish the desired portions of the vascular system from surrounding tissue. Often, only slight changes in the intensity of the image distinguish a desired anatomical structure from surrounding tissue.

Thus, it is desirable to provide a method for isolating anatomical structures of interest such that surrounding tissue is not displayed along therewith. In this manner, the medical diagnostition may view only the unobstructed anatomical structures of interest. This vastly reduces the complexity of the image and thus minimizes confusion as to precisely what portions of the image relate to the anatomical structure of interest.

Summary of the Invention

In the analysis and review of three-dimensional medical imaging, it is of critical importance to be able to measure and analyze image features having various fractal dimensionalities from zero dimensions to three dimensions. For example, veins and arteries are characterized as one-dimensional curvilinear forms, while capillaries exhibit one plus fractal dimensions, typically exhibiting fractional fractal dimensionality. Tumors have three-dimensional fractal forms and exhibit smaller fractal dimensions if metastases are considered.

The present invention specifically addresses and alleviates the above-mentioned deficiencies with the prior art. More particularly, the present invention comprises a method for isolating anatomical structures contained within a three-dimensional data set, e.g., a three-dimensional model formed by MRI, a CAT scan, or a PET scan. The method comprises the steps of forming a morphological skeleton of the three-dimensional data set, selecting a seed data point within the morphological skeleton so as to identify a desired anatomical structure to be displayed or analyzed, and utilizing fuzzy connectivity to define additional data points of the desired anatomical structure so as to reconstruct substantially only the desired anatomical structure. Reconstruction of substantially only the desired anatomical structure facilitates the review and analysis of the anatomical structure.

For example, if it is desirable to obtain a three-dimensional data set containing only data points which are representative of the brain, then the patient's head may be imaged via MRI, CAT, PET scanning techniques or the like to provide a three-dimensional model of substantially the entire head. The three-dimensional data set which defines this model is then processed so as to form a morphological skeleton thereof.

An operator then selects a seed data point within the morphological skeleton corresponding to the patient's brain. This is typically accomplished by viewing the morphological skeleton on a display such as a CRT. The morphological skeleton maintains all of the data available in the original three-dimensional data set. However, in the morphological skeleton, anatomical structures are separated from one another, based upon the fractal dimensionality thereof. Thus, anatomical structures having a fractal dimensionality of less than one dimension are separated from those having a fractal dimensionality of less than two dimensions and the anatomical structures are separated from those having a fractal dimensionality of less than three dimensions.

After selecting a seed data point within the brain, fuzzy connectivity is utilized to define the additional data points which are required to provide a substantially complete image of the brain. Reconstruction of the brain is simply the reverse of the process utilized to form the morphological skeleton. With the use of fuzzy connectivity to define the set of points defining the brain, it appears that all of the features thereof are substantially utilized in the reconstruction process. Reconstruction of the brain without the use of fuzzy connectivity would result in the loss of substantial surface details thereof. For example, the surface texture and even, to a lesser degree, the convolutions of the brain, would tend to be degraded or smoothed.

The morphological skeleton is formed by recursive opening and erosion of the three-dimensional data set so as to form a plurality of residuals which define the morphological skeleton. Reconstructing a desired anatomic structure from the morphological skeleton comprises performing the opposite procedure from that utilized to form the morphological skeleton. Thus, reconstruction

comprises recursive dilation and closing of the morphological skeleton. As those skilled in the art are aware, each step of opening comprises an erosion followed by a dilation and each step of the closing comprises a dilation followed by an erosion.

The use of fuzzy connectivity during the reconstruction process assures that substantially all of the data points associated with the desired anatomical structure are utilized in the reconstruction process.

According to the preferred embodiment of the present invention, a generally spherical structuring element is utilized in both the formation of the morphological skeleton and the reconstruction process. However, those skilled in the art will appreciate that various other shapes of structuring elements are likewise suitable. Indeed, it has been found that various different shapes of structuring elements are particularly suited for use with various different dimensionalities or shapes of anatomical structures.

Generally, the seed data point is selected by positioning a cursor at a desired point on an image being displayed upon a monitor. Thus, the operator may simply visually identify and manually select a seed within the organ or anatomical structure of interest. However, as those skilled in the art will appreciate, various different computer algorithms may be utilized in the selection of such a seed. For example, the operator may simply initiate an algorithm which selects the largest organ within a given volume. Thus, if the operator desires to select the brain for reconstruction, the operator could merely select the largest organ within the head.

The use of fuzzy connectivity to define additional data points of the desired anatomical structure comprises defining connectivity based upon the size and shape of a structuring element utilizing a fuzzy generalization of

mathematically defined distances between sets of data points as a criterion. This is accomplished based upon a modified Hausdorff metric.

Thus, separation of such anatomical features from one another according to the present invention is accomplished via dimensional sieving. Dimensional sieving results in the formation of a morphological skeleton utilizing the recursive opening and erosion processing according to well known principles. The opening and erosion processes are described in detail in "Morphological Systems for Multi-Dimensional Signal Processing" by Petros Maragos and Ronald W. Schafer, Proceeds of the IEEE, Volume 78, No. 4, April 1990; "Morphological Filters-Part I: Their Set-Theoretic Analysis and Relation to Linear Shift-Invariant Filters", by Petros Maragos and Ronald W. Schafer, IEEE Transactions on Acoustics, Speech, and Signal Processing, Volume ASSP-36, No. 8, August 1987; and "Morphological Filters, Part II: Their Relations to Median Order-Statistic, and Stack Filters", by Petros Maragos and Ronald W. Schafer, IEEE Transactions on Acoustics, Speech, and Signal Processing, Volume ASSP-35, No. 8, August 1987.

According to the present invention, a cascade of data dimensional sieving filters are used directly with a three-dimensional image from an MRI device or the like to isolate structures such as arteries and veins from surrounding tissue for unobstructed visualization. This cascade of data dimensional sieving filters comprises the use of a generally spherical structuring element, followed by the use of a two-dimensional surface structuring element, followed by the use of a curvilinear structuring element, followed by the use of a point structuring element.

Thus, to provide for the identification of desired dimensional features within the multi-dimensional data set provided by a tomographic imaging device, a data dimensional sieving algorithm separates the data based upon

the dimensional characteristics of the anatomical structures contained therein. The algorithm utilizes filters which resemble geometric constructions such as lines, disks, and spheres, to sieve multi-dimensional features of curves, surfaces, and regions, as well as features of fractal dimensions in between.

A hierarchy of dimensional filters is thus utilized to first remove features of less than one fractal dimension, then to remove features of less than two fractal dimensions, and finally to remove features of less than three fractal dimensions from the original three-dimensional data set as the morphological skeleton is being formed. Thus, the cascade of filters is used directly with a tomographic image to isolate anatomical structures from surrounding tissues to facilitate analysis and review thereof.

By utilizing the residuals of morphological erosion and opening, the morphological skeleton is formed. This process is ideal for processing data with fractal dimensional components. For example, the recursive formation of the morphological skeleton utilizing alternating opening and erosion transforms a 3.4 dimensional form into .4 dimensional data when a spherical structuring element is utilized.

Once the morphological skeleton has been formed via recursive development utilizing alternating opening and erosion processes, then fuzzy connectivity is utilized in the reconstruction of those anatomical structures of interest. Reconstruction of anatomical structures without utilizing fuzzy connectivity results in the loss of significant features such as surface textures and roughness. These features must be reconstructed from the residuals defining the morphological skeleton utilizing fuzzy connectivity. The reconstruction of such anatomical features requires the satisfaction of a fuzzy connectivity

criteria such that only those tissue features connected to the dimensional features isolated by the sieving process are utilized.

The final result of both the sieving and fuzzy connectivity processes is a classification and clear visualization of the anatomical structures of interest, e.g., tissues and/or tumor pathologies. Additionally, quantification of the volume of organs and tumors as well as other measurements of interest, such as the diameter of arteries and veins, are easily facilitated as a direct result of the use of dimensional sieving and fuzzy connectivity.

Connectivity is a mathematical concept which states that a set of points is connected if and only if every pair of points in the set can be connected by a line which is contained within the set. The algorithm described in this invention generalizes this concept of connectivity to the discrete topological grids utilized by a computer to store the digital image data by utilizing fuzzy set operators. A fuzzy set is itself a generalization of a discrete set by defining a function over a set representing degrees of membership such that membership varies from zero which indicates no membership to one which indicates complete membership.

To define connectivity, this algorithm utilizes a fuzzy generalization of mathematically defined distances between sets as a connectivity criterion. This criterion establishes that if two points or two sets of points are within a specified distance of one another, then they have membership to the same set of points.

The prior art attempted to isolate anatomical features from one another based solely upon the intensity of pixels within the three-dimensional data set. The present invention facilitates the distinguishing or isolation of anatomical features based upon such criteria such as size,

shape, and intensity of the anatomical feature. Thus, more flexibility in designating those features to isolate is provided and improved accuracy of such isolation is attained.

These, as well as other advantages of the present invention will be more apparent from the following description and drawings. It is understood that changes in the specific structure shown and described may be made within the scope of the claims without departing from the spirit of the invention.

Brief Description of the Drawings

Figure 1 is an illustration of the recursive alternating opening and erosion processes for two dimensions utilized to define the residuals of which the morphological skeleton is constructed;

Figure 2 shows the two-dimensional structuring element utilized in the process for forming the morphological skeleton shown in Figure 1;

Figure 3 is a chart giving the results of utilizing structuring elements of different forms or dimensionalities upon images of different forms or dimensionalities;

Figure 4 shows a representative two-dimensional structuring element utilized in the fuzzy connectivity restructuring process wherein 2r is the major diameter thereof;

Figure 5 shows the use of the structuring element of Figure 4 to determine that two points belong to the same set, i.e., a set of data points defining a desired anatomical structure for reconstruction, the two points belong to the same set since when one of the points is located at the center of the structuring element, the other point falls within the bounds defined by the structuring element, wherein the dimension d defines the dimension between adjacent points such that the points fall within

the set;

Figure 6 shows the use of the restructuring element of Figure 4 to iteratively determine that the set points illustrated are contained within a common set;

Figure 7 shows the set support function which defines the degree of fuzzy membership for a given pair of points, which is determined by the modified Hausdorff metric for those points.

Figure 8 is a block diagram of the conventional morphological data decomposition and reconstruction processes;

Figure 9 is a block diagram of the morphological data skeletonization process of the present invention;

Figure 10 is a block diagram of the morphological data decomposition and selective reconstruction processes of the present invention;

Figure 11 is a block diagram of the morphological data dimensional sieving decomposition and selective reconstruction processes utilizing a three-dimension example;

Figure 12 is a block diagram of the morphological data reconstruction from skeleton process of the present invention;

Figure 13 is a block diagram of the morphological data decomposition and selective reconstruction process of the present invention; and

Figure 14 is a block diagram of the fuzzy logic process of the present invention.

Detailed Description of the Preferred Embodiment

The detailed description set forth below in connection with the appended drawings is intended as a description of the presently preferred embodiment of the invention, and is not intended to represent the only forms in which the present invention may be constructed or utilized. The

description sets forth the functions and the sequence of steps for constructing and operating the invention in connection with the illustrated embodiment. It is to be understood, however, that the same or equivalent functions and sequences may be accomplished by different embodiments that are also intended to be encompassed within the spirit and scope of the invention.

The data dimensional sieving and connectivity methodology of the present invention is illustrated in Figures 1-14, which depict a presently preferred embodiment of the invention.

Referring now to Figure 1, the recursive development of a morphological skeleton utilizing alternating opening and erosion process is shown utilizing a two-dimensional geometric construction, i.e., a square, for purposes of illustration. Although a two-dimensional example is provided herein, for purposes as illustration, those skilled in the art will appreciate that use of the present invention in medical imaging typically requires the recursive use of a three-dimensional structuring element such as a sphere, a two-dimensional structuring element such as a surface, a one-dimensional structuring element such as a curve, and a zero-dimensional structuring element, i.e., a point.

After the first opening process, a square 101 having the corners removed therefrom is defined. An octagon 100, as shown in Figure 2, is utilized as the structural element for this example. The corners 102 are the residuals of the opening process for the original square. Each time an additional erosion and opening process is performed, progressively smaller squares 102, 103, and 104 is formed. After each recursive erosion and opening process, additional residuals 102 are defined. After the last erosion process is performed, the square is completely eliminated and the collection of residuals defines the

desired morphological skeleton 106.

Dilation and erosion are defined as follows:

erosion,

$$(g \ominus f_a)(x) = \min_{d \text{ in } E}\{g(x+d) - (f_a(d) - f_a(0))\},$$

dilation,

$$(g \oplus f_a)(x) = \max_{d \text{ in } E}\{g(x+d) + (f_a(-d) - f_a(0))\}$$

$$= - (- g \ominus f_a)(r)$$

Structuring element, f, and image function, g, defined over domain of definition for f, E,

$$f_a(x) = a\, f\left(\frac{x}{a}\right).$$

$$d = \inf\{\, \alpha \mid \inf(X_{\alpha g}) = \sup(X_{\alpha g}), \alpha \in \Re+\},$$

$\alpha g = g(x/\alpha)$, $\Re+$ denotes the real numbers ≥ 0

$$S\varepsilon_{\alpha}(g, X) = (X \ominus \alpha g) - (X \ominus \alpha g)_{+\varepsilon g}, \qquad +0 = \lim_{\varepsilon \downarrow 0} \varepsilon$$

Alternately for a black skeleton the extensive operations of dilation and closing are performed.

$$b = \inf\{\, \alpha \mid \inf(X^{\alpha g}) = \sup(X^{\alpha g}), \alpha \in \Re+\}, \quad \alpha g - g(x/\alpha),$$

$$S\varepsilon_{-\alpha}(g, X) = (X \oplus \alpha g) - (X \oplus \alpha g)_{+\varepsilon} g, \quad \alpha \geq 0$$

For digital raster formats of pixels or voxels, d is limited to the integer domain Z of the data and ε is equal to 1.

$$\Sigma_{\leq \alpha \leq}$$

defined as a single dilation step followed by a single erosion step.

By decreasing the size of the structuring element 100, smaller residuals 102 are obtained and the resolution of the morphological skeleton is increased.

This morphological skeleton contains all of the information contained in the original image. The original image can be reconstructed from the morphological skeleton by reversing the recursive development process, i.e., by substituting dilation and closing for erosion and opening, respectively. Thus, by performing a series of dilations and closings, instead of the openings and erosions performed previously, the original three-dimensional data set is obtained from the morphological skeleton.

In forming the morphological skeleton 102, data dimensional sieving is performed such that anatomical structures having various dimensionalities are separated from one another in a manner which isolates them and makes them identifiable via computational methodology. Thus, according to the methodology of the present invention, those anatomical structures having a fractal dimensionality of less than one dimension are separated from those anatomical structures having a fractal dimensionality of less than two dimensions, both of which are separated from anatomical structures having a fractal dimensionality of less than three dimensions.

A desired anatomical structure which has been so isolated and identified can then be reconstructed by reversing the recursive morphological skeleton development sequence described above utilizing only the data points associated with the selected anatomical structure. However, merely reconstructing the desired anatomical structure results in the loss of significant features such as surface textures and roughness.

Thus, in order to preserve such significant features,

it is necessary to utilize fuzzy connectivity during the reconstruction process. The use of fuzzy connectivity assures that all of the data points associated with the anatomical structure are utilized in the reconstruction process. According to the present invention, fuzzy connectivity defines the entire data set for the desired anatomical structure by utilizing a modified Hausdorff metric, wherein connectivity is defined by the size and shape of the structuring element.

For example, the structuring element is first centered upon a seed pixel by the operator. The seed pixel is one which the operator knows is a part of the anatomical structure for which reconstruction is desired. All other pixels contained within the volume defined by the structuring element are then considered to be a part of the anatomical structure being reconstructed. This process is then repeated for each new pixel within the data set until no additional new pixels are found. Although, as in the formation of the morphological skeleton, many different sizes and shapes of structuring elements are suitable, those generally spherical in configuration are preferred.

A series of different structuring elements may be utilized in either of the formation of the morphological skeleton or the reconstruction process, as desired, so as to achieve a desired effect.

As mentioned above, connectivity is a mathematical concept which states that a set of points is connected if and only if every pair of points in the set can be connected by a line contained in the set. The algorithm described in this invention generalizes this concept of connectivity to the discrete topological grids of computers and digital image data with fuzzy set operators. A fuzzy set is itself a generalization of a discrete set by defining a function over a set representing degrees of membership from no membership as represented by a zero to

complete membership as represented by a one. This algorithm utilizes convex fuzzy membership, as shown in Figure 7, functions defined over convex set supports.

To define connectivity, this algorithm uses a fuzzy generalization of mathematically defined distances between sets as a connectivity criterion. This criterion establishes that if two points or two sets of points are within a specified distance of one another, then they have membership to the same set of points. To more precisely define this concept of connectivity, the neighborhood of points and the data must be defined.

As shown in Figure 7, convexity implies that a line fixed between any two points on the curve of the function must lie on or below the graph of the function:

$$\lambda f(a) + (1 - \lambda) f(b) \leq f(\lambda a + (1 - \lambda)b), \quad 0 \leq \lambda \leq 1$$

erosion,

$$(g \ominus f_a)(x) = \min_{d \text{ in } E} \{g(x+d) - (f_a(d) - f_a(0))\},$$

dilation,

$$(g \oplus f_a)(x) = \max_{d \text{ in } E} \{g(x+d) + (f_a(-d) - f_a(0))\}$$

$$= - (- g \ominus f_a)(r)$$

Structuring element, f, and image function, g, defined over domain of definition for f, E,

$$f_a(x) = a f\left(\frac{x}{a}\right).$$

Minimum Function

$$(g \wedge h)(x) = \min\{g(x), h(x)\}.$$

Maximum function

$$(g \vee h(x) = \max\{g(x), h(x)\}.$$

Based on the previous definitions a measure of distance between sets or points g, h can be defined. This metric is

used to define points or sets within this distance to be fuzzy connected.

2.4.1 Definition: Modified Hausdorff function metric

$$d_f(g,) = \min\Big\{ \alpha \text{ such that } \max_{x \text{ in } E} ((g \wedge h)(x)) < \min_{x \text{ in } E}(((g \oplus f_a) \wedge h \oplus f_a))(x)) \Big\}.$$

Referring now to Figure 3, a chart showing the result of utilizing a structuring element of a particular form or dimensionality on an image of a particular form or dimensionality is shown. The chart includes structuring elements of point, segment, disk, and sphere form and images of point, curve, circles, and volume form. As shown in the chart, utilizing a structuring element defined by a point, for example, in the processing of a curve according to the methodology of the present invention, yields a curve. Similarly, utilizing a segment in the processing of a curve yields a curve and utilizing a disk or sphere in the processing of a curve provides a null product, since a two-dimensional disk or a three-dimensional sphere cannot be utilized to process a one-dimensional curve.

Referring now to Figures 4-6, the use of a two-dimensional example of a structuring element and the fuzzy connectivity reconstruction of a desired anatomical structure is shown. With particular reference to Figure 4, the structuring element 200 shown comprises an ellipse having a major diameter of 2r. Those skilled in the art will appreciate that various other shapes are likewise suitable for use as a structuring element.

Referring now to Figure 5, use of the structuring element to determine if two points are within a common set is shown. This is accomplished by placing the structuring

element 202 around one of the points 210 of interest and then determining whether or not the second point of interest 212 lies within the boundary of the structuring element 202. As shown, the second point 212 does lie within the boundary of the first structuring element 202. In order to find additional points which are part of the common set of points, which define the anatomical structure of interest, this process is repeated by placing a structuring element 204 around the second point 212 in order to determine if any points lie within the boundary thereof.

With particular reference to Figure 6, this process is repeated so as to define all of the points which belong to a common set of data points which define the anatomical structure of interest. Structuring element 202 formed about point 210 defines point 212 as being included within the data set, structuring element 204 formed about point 212 similarly defines point 210 as belonging to the common data set, while structuring element 206 formed about point 212 defines point 214 as belonging to the common data set. Thus, all points which lie within the boundary of any structuring element at which a point within the data set is formed at the center thereof, also are members of the common data set.

Each point so defined to be within the data set is assigned a fuzzy membership number between zero and one, depending upon the distance between adjacent points, as discussed above.

Thus by utilizing fuzzy connectivity, the set of all data points defining a particular anatomical structure of interest are defined such that surface details of the anatomical structure, such as surface smoothness thereof, are maintained during the reconstruction process and are thus included in the reconstructive anatomical structure.

Referring now to Figure 8, an overview of the standard

morphological decomposition and reconstruction process is shown. According to contemporary methodology, an input data array 300 is skeletonized 302 so as to form skeleton 304. Skeleton 304 is then reconstructed 306 so as to provide the original image 308. This process is used in various different data analysis, compression, and data signal processing applications.

Referring now to Figure 9, morphological data skeletonization according to the present invention is shown. Morphological data skeletonization is a recursive process wherein erode image n 320 subjected to erosion 322. The product of erosion is then subjected to dilation 323 and in parallel subjected to erosion 324. The product of erosion 324 is erode image n+1 326 which then becomes new erode image n 320 and is iteratively processed. The product of dilation 323 is subjected to subtraction 325 with respect to erode image in 320 so as to form skeleton 327 which is then subjected to addition with full skeleton 304.

Referring now to Figure 10, morphological data decomposition and selective reconstruction according to the present invention is shown. Input data array 300 is subjected to skeletonization so as to form skeleton 304. Skeleton 304 is used for the selection of a region of interest 310 so as to form edited skeleton 312. Fuzzy connectivity 314 is applied to the edited skeleton 312 to form the edited image 316.

Referring now to Figure 11, a three-dimensional example of the process of morphological data dimensional sieving, decomposition, and selective reconstruction is shown. Input data array 300 is skeletonized 342 wherein a three-dimensional kernel or structuring element configured as a sphere, for example, is utilized in the skeletonization process. The skeletonization 342 results in the formation of a skeleton 343 having less than three-

dimensional features. This skeleton is then subjected to skeletonization 344 utilizing a two-dimensional kernel or structuring element configured as a facette. This two-dimensional skeletonization process 344 results in a skeleton having less than two-dimensional features 345. This skeleton having less than two-dimensional features 345 is then subjected to skeletonization utilizing a one-dimensional kernel or structuring element 346 so as to provide a skeleton having less than one-dimensional features 304.

Referring now to Figure 12, the process of morphological data reconstruction from a skeleton without the use of fuzzy connectivity is shown. As discussed above, such reconstruction results in the loss of substantial surface detail. Using reconstruction n 350, dilation 352 is performed so as to produce dilate image n 353, dilate image n 353 and skeleton n 354 are added 356 and the process is iterated by providing the added images as recon n 350.

Referring now to Figure 13, the process of morphological data decomposition and selective reconstruction of the present invention is shown. Recon n 360 is subjected to dilation 364 so as to produce dilate image n 368 and seed image n 366. Seed image n is subjected to fuzzy connectivity criteria 370 with skeleton n 362 so as to produce edited skeleton 378. Dilate image n 368 is combined 380 with edited skeleton 378 so as to produce a new recon n 360 and the process is iterated.

Referring now to Figure 14, the use of fuzzy connectivity according to the present invention is shown. A seed image n pixel 400 and the skeleton n 402 are operated upon by fuzzy logic 404 utilizing pixel fuzzy logic measure 406, i.e., the selective structuring element, so as to provide pixel fuzzy measure update 408 and set fuzzy connected pixels 410. The use of fuzzy logic in

this manner is described in detail in "Analysis and Segmentation of Higher Dimensional Data Sets With Fuzzy Operators for Representation and Visualization" and published in Neuro and Fuzzy Systems: Emergent Science of Intelligent Computing, by Mitra, Gupta, and Kraske, published by SPIE Press, 1994, ISBN 0-8194-1566-9, provided herewith and forming a part of this patent application, the entire contents of which are hereby incorporated by reference.

Provided below is a list of the symbols utilized in the math equations in this patent application:

Z^n — Module space of integers of dimension n.

$Z+$ — Half space of integers greater than zero.

$\Re^n$ — Euclidean space of real numbers of dimension n.

E — Space domain of which the image is defined over, a Borel field, locally compact, Hausdorff and separable, typically a compact Z^3 or $\Re^3$ space.

Ω — Set of all directions from the center of the unit sphere angles of 4π steradians.

ω — Arbitrary angle within the range of the unit sphere 4π steradians.

r — A point in E of coordinates (x,y,z).

r — A limit point in E of coordinates (x,y,z).

α, d, b — Points on the real line, $\Re$, or integer domain, Z.

d, b — Limit point on the real line, $\Re$, or integer domain, Z.

$d(r1,r2)$ — Euclidean distance between points r1 and r2. $\sqrt{(x1-x2)^2+(y1-y2)^2+(z1-z2)^2}$

B — A structuring element set, compact, convex. symetrical to inversion, with unit radius, $.5 \cdot |B| = 1$.

$|B|$ — Diameter of a set : $\sup \{ d(r1,r2) \mid r1,r2 \in B \}$

B_r — A structuring element set with center translated to point r in the space E.

αB — Scale of the set B by factor α uniformly in all directions relative to the origin of the set coordinate system of definition.

X — A set in the space E or an image defined over E.

X^c — complement of the set X in the space E.

$\varnothing$ — The null or empty set.

$\ominus$ — Image algebraic erosion, Minkowski set subtraction.

$\oplus$ — Image algebraic dilation, Minkowski set addition.

X^B — The closing of a set in the space E or an image defined over E with the structuring element B. $(X \oplus B) \ominus B$.

X_B — The opening of a set in the space E or an image defined over E with the structuring element B. $(X \ominus B) \oplus B$.

$V(\cdot)$ — The measure defined over the space E of functional distributions mapped over the sets of E. A Lebesque measure over continuous space or the sum of voxel intensities over the integer lattice of digital imagery.

$\wedge$ — The infimum of the functional mappings defined over the euclidean space, for integer lattice of digital imagery this corresponds to the minimum of the functional intensity mappings of each voxel.

$\vee$ — The supremum of the functional mappings defined over the euclidean space for integer lattice of digital imagery this corresponds to the maximum of the functional intensity mappings of each voxel.

$/$ — The set difference of binary sets in the euclidean domain or functional difference of mappings over the euclidean domain.

Provided below is a program listing utilized in the practice of the present invention upon a Pixor computer:

```
chmap -i
VolClassify -pat LOWERY -map M mattetable R loweryvent -roi 40 279 38 261 -A Z \
-in 60 -first 4 -name /usr/wolf/data/loweryvent
#chmap -i
#VolClassify -pat LOWERY -map M mattetable R loweryvent -roi 40 279 38 261 -A Z
#       -in 60 -first 4 -name /usr/wolf/data/loweryvent
#chmap -i
# VolClassify -pat LOWERY -map M mattetable R lowerybrain -roi 40 279 38 261 -l
# -A Z -in 60 -first 4 -name /usr/wolf/data/lowerybrain
```

```
#include        "DBM_sizes.h"
#include        "VOX_imagelist.h"
#include        <merge.h>
#include        <math.h>
#include    <vv_impl.h>
#include        <pixar/video.h>
#include        <pixar/chap/pw.h>
#include        <videoreg.h>
#include        <varargs.h>
#include        <sys/time.h>
#include        <sys/stat.h>
#include        "VOXAR.h"

#define PIRL_VOL_NULL           39
#define PIRL_WIN_NULL           40
#define PIRL_TBL_NULL           41

#define INV     DBL2PXL(1.2)

#define mod(a, b)       (((a) < 0)      ? ((b) + (a) % (b)) : ((a) % (b)))

extern  RGBAPixelType   RGBAzero, RGBApoint, RGBAquart, RGBAhalf,
                                                RGBAone, RGBAmax, RGBAinv, RGBAn

extern  COLOR_MATRIX_type       CHANzero, CHANident;

extern  VIDEO   *ThePirlVideo;

extern  double          *make_laplace(), sqrt();

PirlError       VOXVolSkeleton(pv, vol_tbl, thintable, thinscale, thincnt)

PirlPV          *pv;
vol_table_type  *vol_tbl;
RGBAPixelType   *thintable;
double          thinscale;
{       register        thinwidth, thinheight, thindepth, pvdepth, p, threshold;
        register double zspace;
        static  RGBAPixelType   thintable1[4096], growtable[4096], maskrable[409
        static  PirlPV  *skel, *diff, erod, smoothpv;
        static  double  *k, *ka;
        static  TT=5, sum, value;
        static  char    FuncName[] = "VOXVolSkeleton";
        FILE    *fp;

        if((thincnt & 0x3F) != thincnt) thincnt = 0;
        fprintf(stderr, "function %s\n", FuncName);
        if(!pv || !*pv || !vol_tbl || !vol_tbl->vol_link || !thintable)
        {       fprintf(stderr, "%s cannot load a null volume", FuncName);
        CHECK(PIRL_VOL_NULL);
        }
        pvdepth = CountSlices(vol_tbl);
/*      fprintf(stderr, "%s thin scale = %f", FuncName, thinscale);
*/      if(thinscale <= 0. || thinscale > 1.5)  thinscale = 1.5;
        if(thinscale > 1.)      TT=3;   else    TT=5;

        if(!(k = make_3D_sep(k, TT, vol_tbl, thinscale)))
                fprintf(stderr, "kernel cannot be defined");
        dump_sep_kernel(k, TT, stderr);

        fprintf(stderr, "%s volume x = %d y = %d z = %d\n", FuncName,
        (*pv)->xsize, (*pv)->ysize, pvdepth);

        thinwidth = (int)(thinscale * (double)((*pv)->xsize));
        thinheight = (int)(thinscale * (double)((*pv)->ysize));
        zspace = (double)(vol_tbl->slice.pix);
        zspace /= (1000.);
/*      thindepth = (int)(thinscale * (double)((*pv)->zsize));
*/      zspace /= vol_tbl->slice_pos.z - vol_tbl->vol_link->slice_pos.z;
        zspace = (zspace < 0.) ? -zspace : zspace;
```

```
thindepth = (zspace > 1.)
? pvdepth : (int)(zspace*(double)(pvdepth));

CHECK(
PirlCreatePV(&smoothpv, (*pv)->xsize, (*pv)->ysize, pvdepth));
CHECK(
PirlCreatePV(&erod, (*pv)->xsize, (*pv)->ysize, pvdepth));

fprintf(stderr, "%s volume x = %d y = %d z = %d\n", FuncName,
smoothpv->xsize, smoothpv->ysize, smoothpv->zsize);

fprintf(stderr, "%s thin width = %d height = %d depth = %d\n", FuncName,
                                thinwidth, thinheight, thindepth);

for(p = 0; p < 2048; p++)
        if(thintable[p].Alpha)  thintable1[p] = RGBAone;
        else                                  thintable1[p] = RGBAzero

ka=(double *)malloc(27*sizeof(double));
p=27;   while(p--)      ka[p]= k[p/9] * k[(p % 9)/3] * k[p%3];
sum=0;  p=27;   while(p--)      sum += DBL2PXL(ka[p]);
threshold = DBL2PXL(ka[1])-1;
if(threshold <= 8*DBL2PXL(*ka))
fprintf(stderr, "!\t!\t threshold is too LARGE\n");
fprintf(stderr, "threshold minimum = %d\t", 8*DBL2PXL(*ka));
fprintf(stderr, "kernel sum = %d\t", sum);
fp=fopen("kernel.file", "w");
dump_kernel(ka, fp);    fclose(fp);
fprintf(stderr, "threshold = %d\n", threshold);
for(p = 0; p < sum-threshold; p++)                masktable[p] = RGBAzero;
for(p = sum-threshold; p < 2048; p++)   masktable[p] = RGBAone;

for(p = 0; p < threshold; p++)          growtable[p] = RGBAzero;
for(p = threshold; p < 2048; p++)       growtable[p] = RGBAone;

ShowTree(PWStackRoot, FuncName);

CHECK(  VOXFastDumpVolume(pv, NULL));
CHECK(  VOXThreshVolume(pv, thintable1, 0, 0));
/*      if(thinscale > 1.)      {
CHECK(  VOXConvVolKernel(pv, pv, ka));
CHECK(  VOXThreshVolume(pv, growtable, 0, 0));
                        }
*/      CHECK(  VOXCopyVolume(pv, &erod));
p = thincnt;
while(thintable && p--) {
fprintf(stderr, "%s thin count = %d\n", FuncName, p);
CHECK(  VOXCopyVolume(&erod, &smoothpv));
CHECK(  VOXConvVolKernel(&smoothpv, &erod, ka));
CHECK(  VOXThreshVolume(&erod, masktable, 0, 0));
CHECK(  VOXConvVolKernel(&erod, &smoothpv, ka));
CHECK(  VOXThreshVolume(&smoothpv, growtable, 0, 0));
CHECK(  VOXSubVolume(&smoothpv, &erod));
CHECK(  VOXSubVolume(pv, &smoothpv));
                                                }
CHECK(  VOXAddVolume(&erod, &smoothpv));
p = thincnt;
while(thintable && p--) {
fprintf(stderr, "%s thin count = %d\n", FuncName, p);
CHECK(  VOXConvVolKernel(&erod, &smoothpv, ka));
CHECK(  VOXThreshVolume(&smoothpv, growtable, 0, 0));
CHECK(  VOXSubVolume(&smoothpv, &erod));
CHECK(  VOXMultVolume(&smoothpv, pv));
CHECK(  VOXAddVolume(&erod, &smoothpv));
CHECK(  VOXConvVolKernel(&erod, &erod, ka));
CHECK(  VOXThreshVolume(&erod, growtable, 0, 0));
                                                }
p = thincnt;
if(thinscale > 1.)
while(thintable && p--) {
```

```
        fprintf(stderr, "%s thin count = %d\n", FuncName, p);
        CHECK(  VOXConvVolKernel(&erod, &smoothpv, ka));
        CHECK(  VOXThreshVolume(&smoothpv, growtable, 0, 0));
        CHECK(  VOXSubVolume(&smoothpv, &erod));
        CHECK(  VOXMultVolume(&smoothpv, pv));
        CHECK(  VOXAddVolume(&erod, &smoothpv));
        CHECK(  VOXConvVolKernel(&erod, &erod, ka));
        CHECK(  VOXThreshVolume(&erod, growtable, 0, 0));
                                }

        CHECK(  VOXFastReadVolume(pv, NULL));

        CHECK(  VOXMultVolume(pv, &erod));

        CHECK(  PirlDeletePW(&smoothpv));
        CHECK(  PirlDeletePW(&erod));

        return  PIRL_NO_ERROR;
error:  return  PirlLastErr;
}


PirlError       VOXThinVolume(pv, vol_tbl, thintable, thinscale, thincnt)

PirlPV          *pv;
vol_table_type  *vol_tbl;
RGBAPixelType   *thintable;
double          thinscale;
{       register        thinwidth, thinheight, thindepth, pvdepth, p, threshold;
        register double zspace;
        static  RGBAPixelType   thintable1[4096], growtable[4096], masktable[409
        static  PirlPV  origpv, newpv, pvresize;
        static  double  *k;
        static  TT=5, vent_flag=0;
        static  char    FuncName[] = "VOXThinVolume";

        if(thincnt < 0) {       thincnt= -thincnt;      vent_flag=0;    }
        else                    vent_flag=0;
        if((thincnt & 0x3F) != thincnt) thincnt = 0;
        fprintf(stderr, "function %s\n", FuncName);
        if(!pv || !*pv || !vol_tbl || !vol_tbl->vol_link || !thintable)
        {       fprintf(stderr, "%s cannot load a null volume", FuncName);
        CHECK(PIRL_VOL_NULL);
        }
        if(thinscale > 1.)      TT=3;   else    TT=5;
        pvdepth = CountSlices(vol_tbl);
        if(pvdepth > (*pv)->zsize)      pvdepth--;
/*      fprintf(stderr, "%s thin scale = %f", FuncName, thinscale);
*/      if(thinscale <= 0. || thinscale > 2.)   thinscale = 2.;

        if(!(k = make_3D_sep(k, TT, vol_tbl, thinscale)))
                fprintf(stderr, "kernel cannot be defined");

        dump_sep_kernel(k, TT, stderr);

        fprintf(stderr, "%s volume x = %d y = %d z = %d\n", FuncName,
        (*pv)->xsize, (*pv)->ysize, pvdepth);

        thinwidth = (int)(thinscale * (double)((*pv)->xsize));
        thinheight = (int)(thinscale * (double)((*pv)->ysize));
/*      thindepth = (int)(thinscale * (double)((*pv)->zsize));
        zspace = (double)(vol_tbl->slice.pix);
        zspace /= (1000.);
*/      zspace /= vol_tbl->slice_pos.z - vol_tbl->vol_link->slice_pos.z;
        zspace = (zspace < 0.) ? -zspace : zspace;
        thindepth = (zspace > 1.)
        ? pvdepth : (int)(zspace*(double)(pvdepth));

/*      CHECK(
        PirlCreatePV(&origpv, (*pv)->xsize, (*pv)->ysize, pvdepth));
```

```
*/      CHECK(
        PirlCreatePV(&newpv, (*pv)->xsize, (*pv)->ysize, pvdepth));

        fprintf(stderr, "%s new pv width = %d height = %d depth = %d\n", FuncNam
                                                newpv->xsize, newpv->ysize, newp
/*      fprintf(stderr, "%s thin width = %d height = %d depth = %d\n", FuncName,
                                        thinwidth, thinheight, thindepth);
*/
        for(p = 2048; p < 4096; p++)                thintable1[p] = RGBAzero;


        for(p = 0; p < 2048; p++)
                if(thintable[p].Alpha)  thintable1[p] = RGBAone;
                else                                  thintable1[p] = RGBAzero

        threshold = DBL2PXL(k[1] * *k * *k);
        threshold = 256;
        fprintf(stderr, "threshold = %d\n", threshold);
        for(p = 0; p < (2048-threshold); p++)           masktable[p] = RGBAzero;
        for(p = (2048-threshold); p < 2048; p++)        masktable[p] = RGBAone;

        for(p = 0; p < threshold-20; p++)               growtable[p] = RGBAzero;
        for(p = threshold; p < 2048; p++)       growtable[p] = RGBAone;

        CHECK(  VOXCopyVolume(pv, &newpv));
        ShowTree(PWStackRoot, FuncName);

        CHECK(  VOXThreshVolume(&newpv, thintable1, 0, 0));
        p = thincnt;
        while(thintable1 && p--)        {
        fprintf(stderr, "%s thin count = %d\n", FuncName, p);
        CHECK(  VOXSepConvVol(&newpv, &newpv, k, TT));
        CHECK(  VOXThreshVolume(&newpv, masktable, 0, 0));
                                }

        if(vent_flag)   p = thincnt/2;
        else                    p = thincnt;
        while(thintable1 && p--)        {
        fprintf(stderr, "%s thin count = %d\n", FuncName, p);
        CHECK(  VOXSepConvVol(&newpv, &newpv, k, TT));
        CHECK(  VOXThreshVolume(&newpv, growtable, 0, 0));
                                                                        }

        CHECK(  VOXMultVolume(pv, &newpv));

        CHECK(  PirlDeletePW(&newpv));

        return  PIRL_NO_ERROR;
error:  return  PirlLastErr;
}
```

```
#include        "DBM_sizes.h"
#include        "VOX_imagelist.h"
#include        <merge.h>
#include        <math.h>
#include    <vv_impl.h>
#include        <pixar/video.h>
#include        <pixar/chap/pw.h>
#include        <videoreg.h>
#include        <varargs.h>
#include        <sys/time.h>
#include        <sys/stat.h>
#include        "VOXAR.h"

#define INV     DBL2PXL(1.2)

#define PIRL_VOL_NULL           39
#define PIRL_WIN_NULL           40
#define PIRL_TBL_NULL           41

#define mod(a, b)       (((a) < 0)      ? ((b) + (a) % (b)) : ((a) % (b)))

extern  RGBAPixelType   RGBAzero, RGBApoint, RGBAquart, RGBAhalf,
                                                RGBAone, RGBAmax, RGBAinv, RGBAn

extern  COLOR_MATRIX_type       CHANzero, CHANident;


extern  VIDEO   *ThePirlVideo;

extern  double          *make_laplace(), sqrt();

PirlError       VOXProject(in_pv, vol_tbl, perm, angle, range, incr,
                gradtable, recontable, f_name, beam_vol, beamtable)

PirlPV          *in_pv, *beam_vol;
vol_table_type  *vol_tbl;
double          angle, range, incr;
RGBAPixelType   *gradtable, *recontable, *beamtable;
char            *f_name;
{       static  PirlPW  srcpw, ramp_pw, grad_t, grad_m, grad_b, beampw,
                        destpw, pt_pw, scratchpw, prevpw, gradpw, reconpw,
                        shade, shadesub, buf_pw, temp_pw;
        static  RGBAPixelType   *bgtable, *tumortable,
                                                RGBAchan1= { 0x300, 0, 0
        static  double  *k, factor;
        static  coord3D_dbl     g, resize;
        static  char    *line_str, FuncName[] = "VOXProject",
                        filename[128];
        static  rec_width, rec_height,
                        cnt, num_cut, l;
        static  shadeh, shadew, pw_height, pw_width, xoff, yoff;
        int             fd;
        static  struct  {       short   multichannel, width, height, minval, max
                }       FileHeader;

        line_str = malloc(512);
        bgtable=(RGBAPixelType *)malloc(2049*sizeof(RGBAPixelType));
        if(beamtable[800].Red)
        get_mapping_table(bgtable, "beamgrad"); else    bgtable=NULL;
        fprintf(stderr, "executing %s\n", FuncName);
        if(!in_pv || !*in_pv || !vol_tbl || !vol_tbl->vol_link)
        {       CHECK(  PIRL_VOL_NULL);         }
        if(!recontable || !beamtable)
        {       fprintf(stderr, "%s input table is null\n", FuncName);
                goto    noerror;
        }
        if(!gradtable)  gradtable = recontable;
        range += angle;
        fprintf(stderr, "%s angle : initial= %e final= %e increment= %e\n",
                                                FuncName, angle, range,
```

```
factor = (double)(vol_tbl->slice.pix)/1000.;
factor /= (vol_tbl->slice_pos.z - vol_tbl->vol_link->slice_pos.z);
if(factor < 0.) factor = -factor;

switch(perm & VVXYZ)                    {
case VVXZ       :
num_cut = cnt = (*in_pv)->ysize;
pw_width = (*in_pv)->xsize;     pw_height = (*in_pv)->zsize;
rec_width = rec_height = ((*in_pv)->xsize < (*in_pv)->zsize)
? (*in_pv)->zsize : (*in_pv)->xsize;
g.x = 1.; g.y = factor; g.z = 1.;
resize.x = 1.; resize.y = factor; resize.z = 1.;
        break;
case VVYZ       :
num_cut = cnt = (*in_pv)->xsize;
pw_width = (*in_pv)->ysize;     pw_height = (*in_pv)->zsize;
rec_width = rec_height = ((*in_pv)->ysize < (*in_pv)->zsize)
? (*in_pv)->zsize : (*in_pv)->ysize;
g.x = 1.; g.y = factor; g.z = 1.;
resize.x = 1.; resize.y = factor; resize.z = 1.;
break;
default :       perm = VVXY;
case VVXY       :
num_cut = cnt = (*in_pv)->zsize;
pw_width = (*in_pv)->xsize;     pw_height = (*in_pv)->ysize;
rec_height = rec_width = ((*in_pv)->xsize < (*in_pv)->zsize)
? (*in_pv)->zsize : (*in_pv)->xsize;
resize.x = 1.; resize.y = factor; resize.z = 1.;
g.x = 1.; g.y = 1.; g.z = factor;       }

g.x  *= 1.;     g.y  *= 1.;     g.z *= 1.;

shadeh = shadew = (pw_width < pw_height) ? pw_height : pw_width;
xoff = (shadew-pw_width)/2;     yoff = (shadeh-pw_height)/2;

CHECK(  PirlCreatePW(&beampw, pw_width, pw_height, 0));
CHECK(  PirlCreatePW(&buf_pw, (5*rec_width)/4, (5*rec_height)/4, 0));
CHECK(  PirlCreatePW(&destpw, pw_width/4, pw_height, 0));
CHECK(  PirlCreatePW(&grad_m, pw_width/4, pw_height, 0));
CHECK(  PirlCreatePW(&grad_t, pw_width/4, pw_height, 0));
CHECK(  PirlCreatePW(&gradpw, pw_width, pw_height, 0));
CHECK(  PirlCreatePW(&ramp_pw, shadew, shadeh, 0));
CHECK(  PirlCreatePW(&temp_pw, shadew, shadeh, 0));
CHECK(  PirlCreatePW(&scratchpw, pw_width, pw_height, 0));
CHECK(  PirlCreatePW(&shade, shadew, shadeh, 0));
CHECK(
PirlCreateSubPW(&shade, &shadesub, xoff, xoff+pw_width-1,
                                yoff, yoff+pw_height-1, 0xF));
CHECK(  PirlCreatePW(&prevpw, pw_width, pw_height, 0));
CHECK(  PirlCreatePW(&reconpw, rec_width, rec_height, 0));

fprintf(stderr, "%s windows allocated recon width = %d height = %d\n",
                FuncName, rec_width, rec_height);

CHECK(  PirlBeginLines());
CHECK(  PirlSetLineAttributes(line_str, 4., PM_MERGE, &RGBAzero,
                        PE_FELTTIP, 1., PF_SINC, 1.));

if(!(k = make_3D_sep(k, 3, vol_tbl, 1.)))
        fprintf(stderr, "kernel cannot be defined");
else    {       cnt=9;  while(cnt--)    k[cnt] *= 1.5;  }
CHECK(  PirlRampY(ramp_pw, &RGBAmax, &RGBAzero));
do      {

static  coord3D_dbl     light_dir = { -1.2, .6, -.7     }, light, light_
/*      static  coord3D_dbl     light_dir = {   .75, .0, 1.5    }, light;
*/
                static  double  line[6][2];
                coord3D_dbl     resizeT;
                extern  coord3D_dbl     *rotate_vec();
```

```
                    static  PirlPW  subrecon;
                    static  fcnt=0, slice_cnt = 0,
                            xoff1, yoff1, xoff2, yoff2;

    switch(perm)    {
    case VVYZ:      light_a=light_dir;
                            light_a.y= -light_dir.z;        light_a.x= -ligh
                            light_a.z= -light_dir.x;        break;
    case VVXZ:      light_a=light_dir;
                            light_a.y= -light_dir.z;        light_a.x= -ligh
                            light_a.z= -light_dir.y;        break;
    case VVXY:      light_a=light_dir;
                            }
    rotate_vec(&light,&light_a, angle, VVXY);
    fprintf(stderr, "light direction x = %e y %e z %e",
                    light.x, light.y, light.z);
    fprintf(stderr, "rotation angle = %e\n", angle);

    resizeT = resize;
    if(perm & VVZ)
    {       double  tempang;
    tempang = angle*(asin(1.)/90.);
    resizeT.x = resizeT.z = 1.;
    resizeT.y = 1.+(pow(resize.y, 2.)-1.)*pow(sin(tempang), 2.);
    resizeT.y = sqrt(resizeT.y);    }

    fprintf(stderr, "light direction x = %e y %e z %e",
                    resizeT.x, resizeT.y, resizeT.z);

    xoff1 = (int)(rec_width*(1.-resizeT.x))/2;
    yoff1 = (int)(rec_height*(1.-resizeT.y))/2;
    xoff2 = xoff1+(int)(rec_width*resizeT.x)-1;
    yoff2 = yoff1+(int)(rec_height*resizeT.y)-1;

    PirlClear(scratchpw, &RGBAzero);
    CHECK(  VTPutPlane(*in_pv, scratchpw, (*in_pv)->zsize-1,
                            VVXY, VVSINGLE));
    CHECK(  VTPutPlane(*in_pv, scratchpw, (*in_pv)->zsize-2,
                            VVXY, VVSINGLE));
    CHECK(  VTGetPlane(*in_pv, scratchpw, 0,
    perm|((perm & VVZ) ? VVREFLECTX : 0), VVSINGLE));
/*  CHECK(  PirlMulI(scratchpw, &RGBAmax));
*/  CHECK(  VIPMap(scratchpw, scratchpw, VVR, gradtable, 2048));
    CHECK(  VTCompact(scratchpw, grad_t));
    CHECK(
    VTGetPlane(*in_pv, scratchpw, 1,
    perm|((perm & VVZ) ? VVREFLECTX : 0), VVSINGLE));
/*  CHECK(  PirlMulI(scratchpw, &RGBAmax));
*/  CHECK(  VIPMap(scratchpw, scratchpw, VVR, gradtable, 2048));
    CHECK(  VTCompact(scratchpw, grad_m));

    cnt = num_cut;  slice_cnt = 0;
    CHECK(  PirlClear(reconpw, &RGBAzero));
    while(cnt--)    {       double  centerx, centery;
    CHECK(  PirlClear(shade, &RGBAzero));
    CHECK(  VTGetPlane(*in_pv, scratchpw,
    ((3+slice_cnt > num_cut) ? num_cut-1 : 2+slice_cnt),
    perm|((perm & VVZ) ? VVREFLECTX : 0), VVSINGLE));
    CHECK(  VTGetPlane(*beam_vol, beampw,
    ((3+slice_cnt > num_cut) ? num_cut-1 : 2+slice_cnt),
    perm|((perm & VVZ) ? VVREFLECTX : 0), VVSINGLE));
/*  CHECK(  PirlMulI(scratchpw, &RGBAmax));
*/  CHECK(  VIPMap(scratchpw, gradpw, VVR, gradtable, 2048));
    if(bgtable)
    CHECK(  VIPMap(beampw, beampw, VVR, bgtable, 2048));    }
            else
    CHECK(  VIPMap(beampw, beampw, VVR, beamtable, 2048));  }
            CHECK(  PirlAdd(gradpw, beampw));
/*  CHECK(  PirlMerge(beampw, gradpw, beampw, MergeOpBELOW,
```

```
        CHECK(  PirlMulI(beampw, &RGBAmax));
        CHECK(  PirlMulI(beampw, &RGBAmax));
*/
        CHECK(  VTCompact(gradpw, destpw));
        CHECK(  VIPMap(scratchpw, scratchpw, VVR, recontable, 2048));
        CHECK(  VTGetPlane(*beam_vol, beampw,
        ((3+slice_cnt > num_cut)? num_cut-1 : 2+slice_cnt),
        perm|((perm & VVZ) ? VVREFLECTX : 0), VVSINGLET);
        CHECK(  VIPMap(beampw, beampw, VVR, beamtable, 2048));
/*      CHECK(  PirlMerge(scratchpw, beampw, scratchpw, MergeOpPLUS,

        PirlDivI(scratchpw, &RGBAhalf);
*/      CHECK(  PirlAdd(scratchpw, beampw));
        CHECK(  VIPGradient(grad_t, grad_m, destpw, gradpw,
                                g.x, g.y, g.z));
        CHECK(  VIPSurface(prevpw, gradpw, shadesub, 1.2, VVRGBA));
        CHECK(  VIPShade(shadesub, gradpw, shadesub,  light.x, light.y, light.z,
        CHECK(  VIPMap(beampw, temp_pw, VVG, beamtable, 2048));
        if(perm==VVYZ)  {
        CHECK(  PirlCircularShift(temp_pw, -15, -3));
                                        }
        if(perm==VVXY)  {
        CHECK(  PirlCircularShift(temp_pw, 0, 15));
                                        }
        if(beamtable[800].Red)                                          {
        CHECK(  PirlMul(beampw, temp_pw));
        CHECK(  PirlShuffle(beampw, "rrrr"));
        CHECK(  PirlMulI(beampw, &RGBAmax));
        CHECK(PirlAdd(shadesub, beampw));

        CHECK(  PirlClear(temp_pw, &RGBAzero));
        centerx = (double)(shadew/2); centery = (double)(shadeh/2);
        if(light.x > 0.)        line[0][0] = 0.;
        else                            line[0][0] =(float)(shadew-1);
        if(light.y > 0.)        line[0][1] = 0.;
        else                            line[0][1] =(float)(shadeh-1);
        if(light.x != 0. && light.y != 0.)      {       double  magx, magy;

        magx = (light.x > 0.)   ? light.x : -light.x;
        magy = (light.y > 0.)   ? light.y : -light.y;
        if(magx > magy)
        line[0][1] = (float)
                        (centery - (centerx - (double)(line[0][0]))* light.y / l
        else
        line[0][0] = (float)
        (centerx - (centery - (double)(line[0][1])) * light.x /light.y);

        else    if(light.x == 0.)       line[0][0] = (float)centerx;
                        else                                    line[0][1] = (float)cent

        line[1][0]=(float)centerx;      line[1][1] = (float)centery;
        line[1][0] += shade->xmin;      line[0][0] += shade->xmin;
        line[1][1] += shade->ymin;      line[0][1] += shade->ymin;
        line[1][0] = shade->xmax-1;     line[0][0] = shade->xmax-1;
        line[1][1] = shade->ymax;       line[0][1] = shade->ymin;
/*      fprintf(stderr, "line limits x :%e y :%e x :%e y :%e\n",
                        line[0][0], line[0][1], line[1][0], line[1][1]);

        CHECK(  PirlPolyLine(shade, 2, line));
*/      CHECK(  PirlRotate(shade, temp_pw, shade, angle, 1., 1.,
                centerx, centery, 1, 4));
        CHECK(  PirlMul(shade, ramp_pw));
        CHECK(  PirlClamp(shade));
/*      CHECK(  PirlConvolve3x3s(shade, k, k+3));
*/      CHECK(
        VIPProjectOver(shade, reconpw,
        ((perm & VVZ) ? slice_cnt++ : (yoff2-slice_cnt++)), 0,
        (VVNORTH | ((perm & VVZ) ? VVY : VVX)), 1., VVRGBA));
```

```
        pt_pw = scratchpw;      scratchpw = prevpw;     prevpw = pt_pw;
        pt_pw = grad_t; grad_t = grad_m; grad_m = destpw; destpw = pt_pw;
                        }

        CHECK(
        PirlCreateSubPW(&reconpw, &subrecon, xoff1, xoff2, yoff1, yoff2,
        0xF));
        CHECK(  PirlResize(subrecon, reconpw, 4, 4));
        if(vol_tbl->slice_pos.z - vol_tbl->vol_link->slice_pos.z < 0)
        if((perm & VVXY) == VVXY)
        CHECK(  PirlCircularShift(reconpw, 0, -50));    }
        CHECK(  PirlDeletePW(&subrecon));
        CHECK(  PirlResize(reconpw, buf_pw, 4, 4));

/*      ROI_WIDTH(vol_tbl->roi), ROI_HEIGHT(vol_tbl->roi), number_slc));
        if(perm & VVXY)         {
        xshift = ROI_WIDTH(vol_tbl->roi)-(vol_tbl->roi.y2 + vol_tbl->roi.x1);
        xshift /= 2;    xshift = (int)((double)xshift * sin(angle));
                                                }       */

        FileHeader.width = PWXSIZE(buf_pw);
        FileHeader.height = PWYSIZE(buf_pw);
        FileHeader.multichannel = 1;
        sprintf(filename, "%s%02d", f_name, fcnt++);
        fprintf(stderr, "%s\n", filename);
        if((fd = creat(filename, 0644)) < 0)
        {       printf("%s cannot open file %s\n",
                        FuncName, filename);
        }       else    {
        write(fd, &FileHeader, sizeof(FileHeader));
        CHECK(  VIFDCopy(buf_pw, fd, VVRANGE, VVRGBA,
                        0xFC00, 0xBFF,
                        0xFC00, 0xBFF));
        close(fd);
                        }

                }       while((angle += incr), angle < range);

noerror:
        CHECK(  PirlEndLines());
        CHECK(  PirlDeletePW(&scratchpw));
        CHECK(  PirlDeletePW(&grad_t)); CHECK(  PirlDeletePW(&grad_m));
        CHECK(  PirlDeletePW(&destpw)); CHECK(  PirlDeletePW(&shade));
        CHECK(  PirlDeletePW(&reconpw)); CHECK( PirlDeletePW(&gradpw));
        CHECK(  PirlDeletePW(&prevpw)); CHECK(  PirlDeletePW(&temp_pw));
        CHECK(  PirlDeletePW(&buf_pw));

        return  PIRL_NO_ERROR;
error:  return  PirlLastErr;
}
coord3D_dbl     *rotate_vec(light, light_dir, angle, perm)

coord3D_dbl     *light, *light_dir;
double          angle;
{       extern  double  cos(), asin(), sin();

        angle *= (-asin(1.)/90.);
        fprintf(stderr, "light dir x %e y %e z %e\n",
                                        light_dir->x, light_dir->y, light_dir->z
        switch(perm & VVXYZ)    {
        case    VVYZ :
        light->y = light_dir->y * cos(angle) - light_dir->z * sin(angle);
        light->z = light_dir->y * sin(angle) + light_dir->z * cos(angle);
        break;
        case    VVXZ :
        light->x = light_dir->x * cos(angle) - light_dir->z * sin(angle);
        light->z = light_dir->x * sin(angle) + light_dir->z * cos(angle);
        break;
        case    VVXY :
        default :
```

```
        light->x = light_dir->x * cos(angle) - light_dir->y * sin(angle);
        light->y = light_dir->x * sin(angle) + light_dir->y * cos(angle);
                                }

        fprintf(stderr, "light dir x %e y %e z %e\n", light->x, light->y, light-
        return  light;
}
```

It is understood that the exemplary methodology described herein and shown in the drawings represents only a presently preferred embodiment of the invention. As those skilled in the art will appreciate, the present invention is suitable for use in a variety of different applications, other than medical imaging. For example, the present invention may be utilized in radar imaging, machine recognition, and various other imaging applications.

Indeed, various modifications and additions may be made to the described embodiment without departing from the spirit and scope of the invention. For example, various different shapes of structuring elements, other than those illustrated and described, may be utilized in either the morphological skeleton forming process or the reconstruction process. Additionally, various different criteria for defining the present membership of adjacent data points during reconstruction process are likewise suitable. Thus, these and other modifications and additions may be obvious to those skilled in the art and may be implemented to adapt to the present invention for use in a variety of different applications.

Analysis and Segmentation of Higher Dimensional Data Sets with Fuzzy Operators for Representation and Visualization

Wolfgang F. Kraske

Northrop Corporation

Abstract

The segmentation and representation of complex features in higher dimensional data sets is of paramount importance for machine recognition and human perception of image information. A multiresolution and multi–aspect data representation paradigm, a morphological skeleton, is used in this paper to provide a hierarchical framework for efficient representation and visualization of data for machine recognition and human perception of data features. The utilization of fuzzy operators establishes a basis within this framework for organizing packets, or fuzzy sets, of approximate information by minimum coverings or maximal subtence. 3–D and 2–D image data are used to demonstrate applications of these techniques on higher dimensional data sets.

Grayscale mathematical morphology provides an established basis and an algebra for fuzzy operators due to its representation of fuzzy maps over a set support. Specifically, the application of morphological operators in scale and orientation paradigms with tractable support shapes provides an ordered basis for topological analysis and user perception of data. To eliminate precision loss grayscale morphology utilizes only set operations, requiring only computer addition and comparison.

Introduction

The paradigm of the morphological skeleton is introduced for hierarchical organization of fuzzy operators based on resolution. Operator smoothing and differencing operations in L^∞ are exploited to provide multiscale feature representations similar to inner product convolutional basis functions in the L^2 square integrable spaces.

This technique focuses on the specific dimensionalities, and scales of data features. A primary objective of this paper is to present an algorithm which preserves topological morphology and segments delicate and high resolution features to provide a comprehensible representation for machine recognition and human visualization [5, 21]. The fuzzy set algebraic techniques of grayscale mathematical morphology are the basis of this algorithm.

Analysis and Segmentation with Fuzzy Operators for Representation/Visualization

Mathematical morphology offers a multiscale or multiresolution approach for analyzing and segmenting higher dimensional data features across a spectrum of neighborhood scales and resolutions [16,17,22]. Set theory is the underlying concept of mathematical morphology which assumes the representation of data with an open topology such that data analysis with an algebra and topological base of sets is used in contrast to direct analysis of data points [20]. The extension to grayscale mathematical morphology with fuzzy set theory [22,24] facilitates the analysis of data represented as collections of convex functions over an open topological base.

Matheron introduced the algebraic set analysis of mathematical morphology upon binary images to define probability distributions of size and shape spectra relative to a basis of kernel sets or structuring elements [20]. This approach to data representation, as a composition of sets extends to representations of grayscale or fuzzy mappings over sets. This approach deviates from the classical model of higher dimensional data sets perceived as a random and / or discrete collection of numbers or feature vectors to perform cluster analysis upon [8].

For direct applications the algebra of mathematical morphology provides an expression of feature dimensionality and morphology for analysis and classification. In particular the tractability of shape analysis allows the selective study of data features of particular dimensionality and size. Grayscale morphology extends this selectivity to local characteristics with the quantification of texture and gradient as well. The capability of measuring maximum and minimum size extents is also possible by the diametric comparisons of shapes of structuring elements at various scales and orientations. This capability of measuring local intensity and a global morphology of imagery may be particularly beneficial for the quantitative analysis and monitoring of physiological changes in the pathologies of tumors in biomedical imagery and and topographical changes for ariel reconnaissance of evironmental data.

The idea of the spectral distribution of data relative to a basis, such as the Fourier transform is as well supported in the algebra of mathematical morphology with size and orientation distributions to describe images [20,22]. These morphological distributions relate shape information to size and orientation spectra of image data just as the Fourier transform relates spectra of sinusoidal functions to images [17]. Furthermore, the spectral distributions relate to the complexity of describing images with morphological shapes. Simple shapes such as man-made machine parts typically have shape distributions consisting of only a few spectra whereas natural biological structures typically have spectra over a significant range with frequency distributions of the spectra conforming to exponential functions. This function dependence relates to the Hausdorff dimension [10] of fractals [1,9]. The shape characteristic of biological structures is postulated as both a fractal nature [1,9] and a geometric nature [22,23], in fact the Buffon Symposium of 1977 [23] addressed both the topics of fractal synthesis (Mandelbrot) and the morphological analysis (Serra) of biological structures. In retrospect it is therefore plausible from these mutual interests in biomathematics that morphological analysis and fractal synthesis of biological structures are interrelated by a common set theory. The synopsis of this discussion elucidates the philosophy of a broad application and the unifying prospect of morphological analysis suggested in this paper.

2.0 Methods

The primary goal of mathematical morphology has conventionally been the representation of data features by matching sets of particular shape size and orientation, the approach of this

paper is to represent data features as deviations from sets. The selection of the appropriate dimensionality and shape of a structuring element or kernel set for morphological analysis is fundamental to the techniques of this paper. A rigorous development in henceforth developed from topological constructs to operator analysis and finally dimensional filtering.

2.1 Topology and Structuring Elements

The concepts of topology are fundamental to the analysis of image data relative to varieties of sets distinguished by shape, orientation, size and position. The topology used is founded by the norm or families of seminorms on vector spaces. The text of Folland has been an indispensable reference in the development of this formalism [7].

2.1.1 Definition : A vector space X, over a field K, is closed for the following continnous linear mappings given any $\lambda \in K,\ x, y \in X$:

i) vector addition $X \times X \rightarrow X,\ (x, y) \rightarrow x + y\ ,\ \forall\ x, y \in X$.

ii) scalar multiplication $K \times X \rightarrow X,\ (\lambda, y) \rightarrow \lambda y$.

To begin, in particular, sets will be used to analyze images based on neighborhood properties over a vector space X. i.e.

2.1.2 Definition : A topology on X is a family $\mathcal{T}$ of subsets of X with the following properties :

i) $X,\ \emptyset \in \mathcal{T}$

ii) if the cardinality of A, $|A| \leq \aleph = |N|$, and $\{U_\alpha\}_{\alpha \in A} \subset \mathcal{T}$ then $\bigcup_{\alpha \in A} U_\alpha \in \mathcal{T}$.

iii) if $|A| < \aleph$ and $\{U_\alpha\}_{\alpha \in A} \subset \mathcal{T}$ then $\bigcap_{\alpha \in A} U_\alpha \in \mathcal{T}$.

note bene : $|A|$ denotes the cardinality of a set A, N denotes the natural numbers, $|N| = \aleph$.

Hence $\mathcal{T}$ on X defines an topological space $(\mathcal{T}, X)$. This paper will consider topological spaces with countable bases, defining a separable space.

2.1.3 Definition : A **neighborhood base**, $\mathcal{N}(E)$ of $E \subset X$ has the following properties : given a set $\mathcal{V}(E) = \{A : E \subset A,\ A \in \mathcal{T}\}$,

i) $\mathcal{N}(E) \subset \mathcal{V}(E) \subset \mathcal{T}$,

ii) $\forall\ U \in \mathcal{V}(E)\ \exists\ V \in \mathcal{N}(E)$ such that $V \subset U$.

2.1.4 Definition : A base of a topological space $(X, \mathcal{T})$ is a family of sets $\mathcal{B} \subset \mathcal{T}$ such that $\forall\ E \subset X$, $\mathcal{V}(E) \subset \mathcal{B}$ and for any neighborhood base $\mathcal{N}$, of E, $\mathcal{N}(E) \subset \mathcal{B}$.

The consequences of the closure of a topology, $\mathcal{T}$, is considered a Borel σ–algebra is formed. The vector space over this algebra will be the closure of X. This paper will only consider closed vector spaces, denoted as X.

2.1.5 Definition : Given a topological space, $(X, \mathcal{T})$, the closure of $\mathcal{T}$ is a σ – **algebra**, $\mathcal{A}$, such that :

i) $\mathcal{T} \subset \mathcal{A}$, $\overline{X} \in \mathcal{A}$ i.e. $E \in \mathcal{A} \rightarrow E \subset \overline{X}$

ii) $|A| \leq \aleph$, and $\{U_\alpha\}_{\alpha \in A} \subset \mathcal{A}$ then $\bigcup_{\alpha \in A} U_\alpha \in \mathcal{A}$.

iii) $|A| \leq \aleph$, and $\{U_\alpha\}_{\alpha \in A} \subset \mathcal{A}$ then $\bigcap_{\alpha \in A} U_\alpha \in \mathcal{A}$.

(note : If $\overline{X} = X$ then X is complete relative to $\mathcal{T}$, a Banach space)

To simplify analysis of images, restrictions on countable bases $\mathcal{B}$ of $\mathcal{T}$ must be considered. For the image data used in this paper X is an Euclidean vector space, either R^3 or $T^3 = R^3 / \alpha Z^3$, for image size α, if topology is continuous, or Z^3 or Z^3 / nZ^3 if topology is discrete, for image size $n \in Z$. The discrete topologies on Z^3 or Z^3 / nZ^3 have a countable base of points and sets with finite collections of points which defines a separable space. For a continuous space it is necessary to know if a base can be developed from a countable set of scales and translations of an open set, E, with unit radius, R(E) = 1, see below.

2.1.6 Definition : A **seminorm** on a vector space is a mapping $X \rightarrow [0, \infty)$ with the following properties :

i) $p(x + y) \leq p(x) + p(y)$, $\forall x, y \in X$.

ii) $p(\lambda x) \leq |\lambda| p(x)$, $\forall \lambda \in K$, $\forall x \in X$.

if (iii) $p(x) = 0$ iff $x = 0$ then p is a **norm** .

denote $d : X \rightarrow [0, \infty)$ as the **Euclidean norm.**

2.1.7 Definition : A **diameter**, of a set $E \subset X$ is

$$d(E) = \sup\{d(x - y) : x, y \in E\},$$

2.1.8 Definition : A **radius**, of a set $E \subset X$ is

$$R(E) = \inf\{x \in E : \sup\{d(x - y) : y \in E\}\} .$$

Anther set property is now convenient to introduce, the concepts of open sets. Topological spaces in particular are constructions of open sets.

2.1.9 Definition : An **open ball** is a set $B_r(x)$ such that

$B_r(x) = \{y : x, y \in X,\ d(x, y) < r,\ r \in R,\ r > 0\}$,

where d is the Euclidean metric. $B_r(x) \subset X$.

2.1.10 Definition : The interior of a set, $\mathring{A}$, is the union of open balls contained in A,

$$\mathring{A} = \bigcup \{ x \in X : B_{\delta(x)}(x) \subset A, \text{ for some } \delta(x) > 0\}.$$

2.1.11 Definition : An **open set**, U, is a set such that $\mathring{U} = U$.

Given the definition of an open set a more general concept is the definition of a neighborhood.

2.1.12 Definition : A neighborhood, A, of $E \subset X$, is a set such that $E \subset \overset{\circ}{A}$.

With open sets it is now possible to define compact sets, which will complete the introduction of primary topological concepts.

2.1.13 Definition (Heine – Borel) : $K \subset X$ is compact implies that given $K \subset \bigcup_{\alpha \in A} U_\alpha$, where $\{U_\alpha\}_{\alpha \in A}$ is an open collection, $\exists\ D \subset A$, $|D| < \aleph$, such that $K \subset \bigcup_{\alpha \in D} U_\alpha$.

2.1.14 Proposition : If $K \subset X$ is compact then K is bounded , i.e. $K \subset B_r(x)$, for some $r \geq 0$, $x \in X$.

2.1.15 Proposition : If $E \subset R^n$ is bounded and closed then E is compact.

In topological analysis it is convenient to have open sets with an additional bounding property shared by compact sets in vector spaces.

2.1.16 Definition : If E is compact and $E \subset X$ is open then E is precompact hence, $B_{r'}(x) \subset E \subset B_r(x)$, for some $r, r' > 0$, $x \in X$, such that $r' \leq R(E) \leq r$.

Since the analysis of this paper is restricted to countable bases of X, be it R^3 or T^3, the topological properties generated by the translates and scales of a precompact set E are established.

2.1.17 Proposition : A simple base of a topological space $(X, \mathcal{T})$, is a base $\mathcal{B} \subset \mathcal{T}$ such that, $\exists\ E \subset X$, E precompact, $\mathcal{B}_E = \{E_\alpha(\beta) : \alpha \in \Omega,\ \beta \in A\}$, $E_\alpha(\beta) = \alpha E + \beta$, Ω is a countable subset of R, A is a countable subset of X.

Proof. assume $0 \in E$ otherwise choose $x \in E$ and consider $E' = E - x$ which contains $\{0\}$, also assume $R(E) = 1$ otherwise set $E' = \frac{1}{R(E)}E$.

Given $U \subset \mathcal{T}$, $\forall\ x \in U\ \exists\ B_r(x) \subset U$ and for some $r > 0$, $E_{\alpha(x)}(\beta(x)) \in \mathcal{B}$ such that $E_{\alpha(x)}(\beta(x)) \subset B_r(x)$, i.e. $d(x - \beta(x)) \leq \frac{r}{2}$ and $\alpha(x) \leq \frac{r}{2}$, then $U = \bigcup_{x \in U} E_{\alpha(x)}(\beta(x))$, hence $\mathcal{B}_E$ is a base of $\mathcal{T}$.

The condition for a generating set E of a simple base $\mathcal{B}_E$ to be precompact can further be relaxed to include any set assuming the second condition of the Baire category theorem is satisfied, hence this theorem is stated below. First the definition of a dense set is required.

2.1.18 Definition : If $A \subset X$, then A is dense relative to X if $\overline{A} = X$.

2.1.19 Baire Category Theorem : Let X be a complete metric space.

i) If $\{U_n\}_{n\in N}$ is a countable collection of open dense subsets in X then $\bigcap_{n\in N} U_n$ is dense in X.

ii) if $X = \bigcup_{n\in N} E_n$ then for some $k \in N$, $\overline{E}_k$ is a neighborhood of some point in X. $\overline{E}_k$ is the closure of E_k .

These generating sets of the simple base of a topology are commonly referred to as structuring elements in mathematical morphology. To reduce complexity of analysis these structuring elements are further restricted to be convex as well as precompact.

2.1.20 Definition : $E \subset X$ is convex then $\forall\, x,\ y \in E$,

$$\lambda x + (1 - \lambda)y \in E,\ \forall\, \lambda \in [0,1].$$

Given a precompact convex set E several properties useful for further developments in functional analysis will be characterized. The following mathematical formalism for convex function spaces has been extended from that established by Conway [3] .

2.1.21 Proposition : given a precompact − convex set E
$\exists$ a unique point $c \in \overline{E}$ from which the radius of $\overline{E}$ can be defined, $E \subset B_{R(c)}(q)$.
Denote this point c as the center of Radius of E.

Proof. consider $R_x(E) = \sup\{d(x - y) : y \in E\}$,
since $R(E) = \inf\{R_x(E) : x \in E\}$ $\exists\, x \in \overline{E}$
such that $R_x(E) = R(E)$.
Suppose $R_p(E) = R_q(E) = R(E)$ with $q \neq t$, $q, t \in \overline{E}$.
Hence $\forall\, x \in E$, $d_t(x)$, $d_t(x) < R(E)$, where $d_t(x) = d(t - x)$.
This implies that $E \subset B_R(q) \cap B_R(t)$,
But $E \subset B_R(q) \cap B_R(t) \subset B_{R'}(\bar{x})$, $\bar{x} = \frac{t + q}{2}$.
$(R')^2 = R^2 - \left(\frac{t - q}{2}\right)^2 < R^2$,
$\bar{x} \in \overline{E}$ since E is convex and $R(E) \leq R_x(E) < R(E)$
with $q \neq t$, a contradiction. Therefore $q = t = c$.

Furthermore if E is has a sufficient number of axes of symmetry the unique center of radius is a member of the precompact structuring element E.

2.1.22 Proposition : if a precompact − convex set E has hyperplanes of symmetry $\{P_i\}_{i=1}^{N}$ with a unique point of intersection, c, this point is both in E and center of radius of E, $R_c(E) = R(E)$.

Proof. given $P \in \{P_i\}_{i=1}^{N}$, By symmetry property if $x \in E$ then $\exists\, x' \in E$ such that x' is the reflection of x across P, i.e. $\bar{x} = \frac{(x + x')}{2} \in P$,
$\bar{x} = \rho_P(x) = \inf\{d(x - y) : y \in P\}$.
Hence if c is center of radius of E, $R(E) = R_c(E)$, then the reflection of c across P, c' is also a center of radius of E $R_{c'}(E) = R_c(E)$, by the previous proposition 2.1.21 c is unique and $c = c'$, by symmetry this implies $c \in P$. But $P \in \{P_i\}_{i=1}^{N}$ is arbitrary hence $c = \bigcap_{i=1}^{N} P_i$ a unique point.
Now choose $x \in E$ with $x \neq c$ this implies that $x \notin P \in \{P_i\}_{i=1}^{N}$, from above x', and $\rho_P(x) \in E$.
By induction $c = \left(\prod_{i=1}^{N} \rho_{P_i}\right)(x) \in E$.

The structuring element is selected to resemble the compact neighborhood form of the data structures of interest. For fractal data this is particularly convenient since the same primitive form and structure may be repeated over a broad range of scales. Hence the selected structuring element forms will locally resemble the features of interest in compact neighborhoods. Therefore, a compact 3–D sphere and 1–D arbitrarily oriented line segment are selected for biomedical imagery as structuring elements to represent the neighborhood of brain surface structures and vascular curvilinear structures respectively. The data analysis of complex image features with compact and convex structuring elements is easily implemented on parallel processing digital computers.

To demonstrate the shape of the approximate spherical structuring element, note that the structuring element in Figure 1 is eight sided and symmetrical in two sets of four directions. Note that the lines of symmetry of this structuring element require the center of radius to be within the structuring element, proposition 2.1.22. This shape possesses a quality of directional isotropy which is ideal for size and convexity analysis of 3–D image features however it is likewise not disposed to provide an analysis of the orientation of image features. Further analysis of the curvilinear features of 1–D forms, such as the arteries and veins of 3–D MRA acquisitions, requires oriented structuring elements resembling 1–D line segments such as elongated ellipses. Symmetry about a central point is common property of all structuring elements used in this paper and thus the coordinate system of the structuring element originates from this central point, or center of radius.

Since images are functions mapped over a complete vector space, a Banach space, X, [3,7] the development the above formalisms of set analysis must be extended to the representation of functions mapped over X. In discrete topologies with a countable base however, a sphere and other continuous space sets cannot exist in a digital representation. Hence the structuring element applied in this paper digitally approximates a sphere

A convex function, g, will be introduced in the next section, mapped over the structuring element domain to extend the topological basis to a functional basis. If g is non–constant over the basis support then the structuring element boundaries are fuzzified, permitting more precise approximation of a sphere and greater flexibility with generalization in data analysis.

Analysis and Segmentation with Fuzzy Operators for Representation/Visualization

Several generalizations of the set basis definitions are now presented for positive function mappings over the basis set, primarily, the structuring element diameter and radius will be that of the support.

2.1.23 definition : the **diameter** of a positive mapping
g is $d(g) = \sup \{d(x - y) : g(x),\ g(y) > 0\}$.
Assume $d(g) = 2$ for g unless otherwise stated.

2.1.24 definition : the **radius** of a positive mapping g is,
$R(g) = \inf\{\sup \{d(x - y) : g(y) > 0\} : g(x) > 0\}$.
Assume $R(g) = 1$ for g unless otherwise stated.

2.2 Fundamental Algebraic Operations

There are two primary neighborhood operations of mathematical morphology, which are related by set complementation and are critical for the analysis and development of the morphological representation. These operations are dilation and erosion. Conveniently the homogeneous cascade of these neighborhood operations increases the scale of the structuring element without precision loss. To perform these critical operations of dilation and erosion the structuring element must be translated over the image domain. To formulate these operations a definition of the functions and the bases which support the analysis of these functions must be derived. The approach of this development is to extend the developments of the last section to function bases which provide analysis of function or image mappings in higher dimensional vector spaces X. Dilation is defined with properties proved and then its dual operation of erosion is introduced.

2.2.1 Definition : g is a convex mapping over E, $E \in \mathcal{E}_E$,
where E is a compact convex generating set of $\mathcal{E}_E$.

$$\mathcal{B}_g = \{g_A + \beta : \beta \in \Omega,\ A \in \mathcal{E}_E\}$$

For ease of notation $\alpha g = g_{\alpha E}$,
i.e. $\alpha g\left(\frac{1}{\alpha}x\right) = g_{\alpha E}(x) \quad \forall\ x \in E$.
hence, $\alpha g(\alpha 0) = g_{\alpha E}(0) = g_E(0)\ \forall\ \varepsilon > 0$.

With the basis, $\mathcal{B}_g$, the objective is to approximate functions to arbitrarily precision in the space of L^∞ functions with Lebesque measure over the topological vector space $(X,\mathcal{T})$.

2.2.2 If $f: X \to K$ where $K = R, Z$,
Consider $C^a f = \{x : x \in X,\ |f| > a\}$, furthermore
since f is a function if $a > b$, $C^a f \subset C^b f$,
then $|f|_\infty = \inf\{a \geq 0 : m(C^a f) = 0\}$,
alternately, $|f|_\infty = \sup\{a \geq 0 : m(C^a f) > 0\}$,
m is the Lebesque measure on $(X,\mathcal{A})$, if $f \in L^\infty$ then $|f|_\infty < \infty$.

note : to simplify notation assume $|f| = |f|_\infty$.

A more general class of functions can be admitted if these functions are considered integrable over precompact neighborhoods.

2.2.3 **definition** : $f \in L^\infty_{loc}$ implies $\forall$ precompact $U \subset X$,

$|f|_U = \inf\{a \geq 0 : m(C^a_U f) = 0,\ U \subset U' \in \mathcal{T}\}$,

where $C^a_U f = U' \cap C^a f$.

Without loss of generality f can be restricted to a positive function over X. It can now be shown that the set base, $\mathcal{B}_E$, can approximate a function, f, arbitrarily closely in the L^∞ norm. The results will then be shown to extend to using the function base, $\mathfrak{B}_g$.

2.2.4 given $F \subset X$, the **measure** of F is :

$$m(F) = \inf\{m(U) : F \subset U \in \mathcal{T}\} .$$

Using the L^∞ norm there exists a mapping of L^∞_{loc} into the set of upper semi–continuous functions, $\mathcal{U}$, with function bases, $\mathfrak{B}_g$, supported by the the precompact topological bases, $\mathcal{B}_E$, of section 2.1.

2.2.5 **definition** : If $f \in \mathcal{U}$, $f : X \to K$, then

$f^{-1}((-\infty, a))$ is open in X $\forall$ a $\in$ K.

To facilitate further development a new function will be defined.

2.2.6 **definition** : $f^x_{g_t} = \left(f + \hat{g}^x_t\right) \chi_{\text{supp } \hat{g}^x_t}$, where χ_B is the characteristic function :

$$\chi_B(x) = \begin{cases} 1 & , \text{ if } x \in B \\ 0 & , \text{ if } x \notin B \end{cases} , \quad \text{for } B \subset X .$$

The most fundamental operation for the image analysis developed in this paper is now introduced, the dilation mapping relative to a structuring element E.

2.2.7 **definition** : A **dilation** mapping, Γ, performs the following operation :

$$\Gamma^g_t f(x) = |f^x_{g_t}| - \varepsilon, \quad \sup_{y \in \hat{E}_t(x)} \hat{g}^x_t(y) = \hat{g}^x_t(0) = \varepsilon. \qquad (1)$$

$\hat{E}_t(x)$ is the reflection of $E_t(x)$ about x.
Likewise $\hat{g}^x_t$ is the reflected mapping of $\hat{g}^x_t$ about x
with $\hat{E}_t(x)$ the support of $\hat{g}^x_t$.

note : the analysis of this paper will use symmetric $\hat{g}^x_t$ such that, $\hat{g}^x_t = g^x_t$.

Denote Γ^g_t as Γ_t if the structuring element g is understood.

The introduction of the function mapping of dilation permits the proof of several interesting results for image analysis : extendibility, continuity and order preservation of $\mathcal{U}$.

2.2.8 proposition :

i) $\Gamma_\varepsilon f \geq \Gamma_{\varepsilon'} f$ if $\varepsilon \geq \varepsilon'$.

ii) $\Gamma_\varepsilon f(x)$ is continuous with respect to ε, $\forall\, \varepsilon > 0,\ x \in X$.

proof :

(i) $\hat{g}^x_\varepsilon(y) \geq \hat{g}^x_{\varepsilon'}(y)\ \forall\, y \in X$, if $\varepsilon \geq \varepsilon'$,

since g is convex,

hence, $f^x_{\varepsilon g} \geq f^x_{\varepsilon' g}$, for $f^x_{\varepsilon g} = \left(f + \hat{g}^x_\varepsilon\right) \chi_{\operatorname{supp} \hat{g}^x_\varepsilon}$,

$\Gamma_\varepsilon f(x) = \left|f^x_{\varepsilon g}\right| - \varepsilon$, where $\hat{g}^x_\varepsilon(0) = \varepsilon$,

$\geq \sup\left\{\left|f^x_{\varepsilon g}\right|_{\lambda_\varepsilon(x)},\ \left|f^x_{\varepsilon g}\right|_{\lambda_{\varepsilon'}(x)}\right\} - \varepsilon$,

$A_\varepsilon(x) = E_\varepsilon(x) \setminus E_{\varepsilon'}(x),\ \varepsilon \geq \varepsilon'.$

$\geq \left|f^x_{\varepsilon g}\right|_{\hat{E}_{\varepsilon'}(x)} - \varepsilon$

$\geq \left|f^x_{\varepsilon' g}\right|_{\hat{E}_{\varepsilon'}(x)} - \varepsilon = \left|f^x_{\varepsilon' g}\right| - \varepsilon = \Gamma_{\varepsilon'} f(x)$

Therefore, $\Gamma_\varepsilon f \geq \Gamma_{\varepsilon'} f$ since $\Gamma_\varepsilon f(x) \geq \Gamma_{\varepsilon'} f(x)\ \forall\, x \in X$.

(ii) $\Gamma_\varepsilon f$ is continuous from bellow :

$\sup\left\{\Gamma_b f(x) + b : b < \varepsilon\right\}$

$= \sup\left\{\sup\left\{a \geq 0 : m\left(C^a f^x_{\varepsilon g}\right) > 0\right\},\ b < \varepsilon\right\}$

$= \sup\left\{a \geq 0 : m\left(C^a f^x_{\varepsilon g}\right) > 0\right\}$, since $f^x_{\varepsilon g} \geq f^x_{b g}$ for $\varepsilon > b$,

$= \Gamma_\varepsilon f(x) + \varepsilon$.

or ,

$$\Gamma_\varepsilon f(x) = \sup\left\{\Gamma_b f(x) : b < \varepsilon\right\} .$$

$\Gamma_\varepsilon f$ is continuous from above :

$\inf\left\{\Gamma_b f(x) + b : b > \varepsilon\right\}$

$= \inf\left\{\inf\left\{a \geq 0 : m\left(F_a\left(C^a f^x_{b g}\right)\right) = 0\right\},\ b > \varepsilon\right\}$

$= \inf\left\{a \geq 0 : m\left(C^a_{E_\varepsilon(x)} f^x_{b g}\right) = 0\right\}$,

i.e. $\overline{E_\varepsilon(x)} = \bigcap_{b<\varepsilon} E_b(x)$, $E_b(x) = \operatorname{supp}\left\{f^x_{b g}\right\}$,

$= \inf\left\{a \geq 0 : m\left(C^a_{E_\varepsilon(x)} f^x_{b g}\right) = 0\right\}$

$= \left|f(x)\right|_{\overline{E_\varepsilon(x)}} = \sup\left\{\left|f(x)\right|_{E_\varepsilon(x)},\ \left|f(x)\right|_{\partial E_\varepsilon(x)}\right\}.$

$= \left|f(x)\right|_{E_\varepsilon(x)} = \Gamma_\varepsilon f(x) + \varepsilon$.

or ,

$$\Gamma_\varepsilon f(x) = \inf\left\{\Gamma_b f(x) : b > \varepsilon\right\} .$$

By definition the basis functions of $\mathfrak{B}_g$ are bounded convex mappings over a precompact convex support. With definitions of a norm it is now possible to develop a norm with respect to the convex neighborhood properties of the support of g, i.e. E = supp g is convex.

2.2.9 definition : A set E is balaced if $\beta x \in E$, whenever $x \in E$, and $|\beta| \leq 1$, for $\beta \in K$.

A balanced set implies symmetry of the set about any hyperplane through the origin. Hence a precompact–convex structuring element set which is balanced contains its center of radius, which is as well a center of symmetry, as specified by proposition 2.1.22.

2.2.10 proposition : Given a precompact, convex and balanced set $E \subset X$, $\{0\} \in E$, then

$$p_E(x) = \inf\{\lambda : x \in \lambda E\} \text{ , is a norm on X.}$$

proof. Given a precompact – convex set, $E \subset X$, the three properties of the norm are to be demonstrated.

i) $p_E(x) = \inf\{\lambda > 0 : x \in \lambda E\} \geq 0 \; \forall \; x \in X$ since
$\exists \; \delta > 0, \; 0 \in B_\delta(0) \subset E$, and $\frac{\delta}{d(x) + \varepsilon} x \in B_\delta(0)$,
or $x \in \frac{d(x) + \varepsilon}{\delta} E$ for any $\varepsilon > 0$ and $\forall \; x \in X$.
therefore $0 \leq p_E(x) \leq \frac{d(x)}{\delta} \; \forall \; x \in X$ and $p_E(x) = 0$ iff $x = 0$.

ii) $p_E(\beta x) = \inf\{\lambda > 0 : \beta x \in \lambda E\}$

$$= |\beta| \inf\left\{\frac{\lambda}{|\beta|} > 0 : x \in \frac{\lambda}{|\beta|} E\right\} = |\beta| p_E(x)$$

$\forall \; \beta \in K - \{0\}$.

If $\beta = 0$, $\beta x = 0$ and $p_E(\beta x) = 0$ by (i).
n.b. that if $\beta \geq 0$, the balanced set condition can be relaxed.

iii) Given $x, y \in X$, $\varepsilon > 0$,

$x' = \frac{x}{p_E(x) + \varepsilon}$, $y' = \frac{y}{p_E(y) + \varepsilon} \in E$ since $p_E(x')$, $p_E(y') < 1$.
Using the convexity of E with $\eta \in [0, 1]$,
then $\eta x' + (1 - \eta) y' \in E$, and $p_E(\eta x' + (1 - \eta) y') < 1$.
Now suppose

$$\eta = \frac{p_E(x) + \varepsilon}{p_E(x) + p_E(y) + 2\varepsilon} \text{ then by (ii)}$$

$p_E(x + y) < p_E(x) + p_E(y) + 2\varepsilon$, but ε is arbitrary,
hence $p_E(x + y) < p_E(x) + p_E(y) \; \forall \; x, y \in X$.

This norm in X, proposition 2.2.10, can now be extended to convex mappings over these pre-compact–convex–balanced sets.

2.2.11 Theorem : Given a decreasing convex mapping, h, over $p_E(x)$, $h : [0, 1] \rightarrow [0, 1]$, $h(0) = 1$, the composition $g = h \bigcirc p_E$ is a convex mapping over E, with the property ,

$$\varepsilon g\left(\frac{x}{\varepsilon}\right) + \eta g\left(\frac{y}{\eta}\right) \leq (\varepsilon + \eta) g\left(\frac{x + y}{\varepsilon + \eta}\right) , \quad \forall \; \varepsilon, \; \eta > 0,$$

$x \in \varepsilon E, \; y \in \eta E$.

proof. Given a precompact − convex set $E \subset X$,

$$\varepsilon g\left(\frac{x}{\varepsilon}\right) + \eta g\left(\frac{y}{\eta}\right) = (\varepsilon + \eta)\left(\varepsilon' h\left(\frac{p_E(x')}{\varepsilon'}\right) + \eta' h\left(\frac{p_E(y')}{\eta'}\right)\right),$$

where $\varepsilon' = \frac{\varepsilon}{\varepsilon + \eta}$, $\eta' = 1 - \varepsilon'$, $x' = \frac{x}{\varepsilon + \eta}$, $y' = \frac{y}{\varepsilon + \eta}$,

now $\varepsilon' h\left(\frac{p_E(x')}{\varepsilon'}\right) + \eta' h\left(\frac{p_E(y')}{\eta'}\right) \le h(p_E(x') + p_E(y'))$,

since h is convex.
By prop. 2.2.11 $p_E(x') + p_E(y') \ge p_E(x' + y')$,
combined with the decreasing property of h,
$h(p_E(x') + p_E(y')) \le h(p_E(x' + y')) = g\left(\frac{x + y}{\varepsilon + \eta}\right)$.
hence, $\varepsilon g\left(\frac{x}{\varepsilon}\right) + \eta g\left(\frac{y}{\eta}\right) \le (\varepsilon + \eta) g\left(\frac{x + y}{\varepsilon + \eta}\right)$.
This property of g implies g is convex.
Since $p_E : E \to [0, 1]$ and $h : [0, 1] \to [0, 1]$,
then $g = h \circ p_E : E \to [0, 1]$.

2.2.12 corollary : Given g a convex mapping over E
$\Gamma_{\varepsilon'} g_\varepsilon + \varepsilon' = \Gamma_\varepsilon g_{\varepsilon'} + \varepsilon = g_{\varepsilon+\varepsilon'}$.

proof. Since g is convex g is continuous, hence

$$\Gamma_{\varepsilon'} g_\varepsilon(x) + \varepsilon' = \sup\left\{\varepsilon' g\left(\frac{y}{\varepsilon'}\right) + \varepsilon g\left(\frac{x - y}{\varepsilon}\right) : y \in E_{\varepsilon'}\right\}$$
$$= (\varepsilon' + \varepsilon) g\left(\frac{x}{\varepsilon + \varepsilon'}\right) = g_{\varepsilon+\varepsilon'}(x), \text{ by theorem.}$$

Therefore $\Gamma_{\varepsilon'} g_\varepsilon(x) + \varepsilon' = g_{\varepsilon+\varepsilon'}(x)$.

2.2.13 Lemma : Given $\varepsilon' - \varepsilon = \delta > 0$ and $f \in L^\infty_{lsc}$,
then $\Gamma_\varepsilon f(y) \le \Gamma_\varepsilon f(y) + \hat{g}^x_\delta(y) \le \Gamma_{\varepsilon'} f(x) + \delta$, $\forall\, y \in E_\delta(x)$.

proof. If $f \in L^\infty_{lsc}$ and $\varepsilon' > \varepsilon$ then $\Gamma_\varepsilon f(x) \le \Gamma_{\varepsilon'} f(x)$,
by (i) prop. 2.2.8.
Set $\varepsilon' - \varepsilon = \delta > 0$ and choose any $y \in E_\delta(x)$
then $\hat{g}^z_\varepsilon + \hat{g}^x_\delta(y) \le \hat{g}^z_{\varepsilon'}$ by prop. 2.2.11, hence $f^z_{\varepsilon\varepsilon} + \hat{g}^x_\delta(y) \le f^z_{\varepsilon'\varepsilon}$,
which implies $\lfloor f^z_{\varepsilon\varepsilon} \rfloor + \hat{g}^x_\delta(y) \le \lfloor f^z_{\varepsilon'\varepsilon} \rfloor$ and
$\Gamma_\varepsilon f(y) + \hat{g}^x_\delta(y) - \delta \le \Gamma_{\varepsilon'} f(x)$.

2.2.14 Theorem : $\Gamma_\varepsilon : L^\infty_{lsc} \to \mathcal{U} \subset L^\infty_{lsc}$ $\forall\, \varepsilon > 0$.

proof. If $\Gamma_\varepsilon f \in \mathcal{U}$ for $f \in L^\infty_{lsc}$ then
$A^a \Gamma_\varepsilon f = \{x \in X : \Gamma_\varepsilon f(x) < a\}$ is open in X.
Choose $x \in A^a \Gamma_\varepsilon f$ then $\Gamma_\varepsilon f(x) < a$:
Choose $\varepsilon' > \varepsilon$ then $\Gamma_\varepsilon f(y) \le \Gamma_{\varepsilon'} f(x) + \delta$,

for any $y \in E_\delta(x)$ and $\varepsilon' - \varepsilon = \delta > 0$, by (i) lemma 2.2.13 .
Choose δ small enough such that $\Gamma_\alpha f(x) + \delta < a$,
and hence $\Gamma_\alpha f(y) < a$, $\forall\, y \in E_\delta(x) \subset A^a\, \Gamma_\alpha f$.
Since $x \in A^a\, \Gamma_\alpha f$ was chosen arbitrarily this
implies that $A^a\, \Gamma_\alpha f$ is open and $\Gamma_\alpha f \in \mathfrak{U}$.
Furthermore since $f \in L^\infty_{loc}$ is arbitrary it is shown
$\Gamma_\alpha : L^\infty_{loc} \to \mathfrak{U} \subset L^\infty_{loc}$ $\forall\, \varepsilon > 0$.

The now formally introduced image transformation of dilation not only projects the function space L^∞ into the upper semicontinuous functions but restricts the neighborhood mapping properties of these functions.

2.2.15 Definition : If $f \in \mathfrak{U}$ then $\lim_{\alpha \to 0} \Gamma_\alpha f = f$.

2.2.16 Lemma : Given $f \in \mathfrak{U}$, $\varepsilon > 0$, then $\forall\, x \in X$,

$$\Gamma_\alpha f(x) = \sup\{f^\varepsilon_{g_\alpha}(y) : \; y \in E_\alpha(x)\} - \varepsilon \; .$$

proof. Suppose $f \in \mathfrak{U}$ then by prop. 2.2.13 $\forall\, x \in X$,

$$\Gamma_\alpha f(x) + \delta \geq \sup\{\, \Gamma_{\alpha-\delta} f(y) : \; y \in E_\delta(x)\} \; ,$$

hence $\Gamma_\alpha f(x) + \varepsilon \geq \sup\{\, f(y) : \; y \in E_\alpha(x)\}$.
But since $f^\varepsilon_{g_\alpha}(y) - \varepsilon \leq f(y)$,

$$\Gamma_\alpha f(x) \geq \sup\{\, f^\varepsilon_{g_\alpha}(y) - \varepsilon : \; y \in E_\alpha(x)\}$$
$$\geq |\, f^\varepsilon_{g_\alpha}| - \varepsilon = \Gamma_\alpha f(x) \; ,$$

hence $\Gamma_\alpha f(x) = \sup\{\, f^\varepsilon_{g_\alpha}(y) - \varepsilon : \; y \in E_\alpha(x)\}$.

2.2.17 Lemma : Given $f \in L^\infty_{loc}$, $\varepsilon > 0$, then

$\Gamma_\alpha f = \Gamma_\alpha \hat{f}$, where $\hat{f} = \lim_{\alpha \to 0} \Gamma_\alpha f \in \mathfrak{U}$.

proof. (a) If $f \in L^\infty_{loc}$ then by definition 2.2.7,
$\Gamma_\alpha f \geq f + \hat{g}^\varepsilon_\alpha - \varepsilon$ on $E_\alpha(x)$ a.e.
where a.e. means almost everywhere except on a subset of $E_\alpha(x)$
of measure (definition 2.2.4) zero . Hence
$\hat{f}(x) = \lim_{\alpha \to 0} \Gamma_\alpha f \geq \lim_{\alpha \to 0} \{f(y) + \hat{g}^\varepsilon_\alpha(y) - \varepsilon,\; y \in E_\alpha(x)\}$ a.e. ,
therefore $\hat{f} \geq f$ a.e. and $\Gamma_\alpha \hat{f} \geq \Gamma_\alpha f$ for all $\alpha > 0$.

(b) Now suppose $x \in X$ such that $\Gamma_\alpha \hat{f}(x) > \Gamma_\alpha f(x)$,
Then by lemma 2.2.16 , $\exists\; y \in E_\alpha(x)$ such that

$$\Gamma_\alpha \hat{f}(x) \geq \hat{f}^\varepsilon_{g_\alpha}(y) - \varepsilon = \hat{f}(y) + g^\varepsilon_\alpha(y) - \varepsilon > \Gamma_\alpha f(x) \; ,$$

but by lemma 2.2.13 $\hat{f}(y) + g^\varepsilon_\alpha(y) \leq \Gamma_\alpha f(x) + \varepsilon$,
a contradiction,
Therefore (a) combined with (b) implies $\Gamma_\alpha \hat{f}(x) = \Gamma_\alpha f(x)$.

2.2.18 proposition : given the dilation mappings Γ_ε, $\Gamma_{\varepsilon'}$, constructed with the convex structuring element g , the composition map has the property :

$$\Gamma_{\varepsilon'}\Gamma_\varepsilon f = \Gamma_{\varepsilon'+\varepsilon} f \quad \forall f \in L^\infty_{loc} . \tag{2}$$

proof. Suppose $f \in L^\infty_{loc}$ then by lemma 2,2,17, $\forall\, x \in X$,
$\Gamma_\varepsilon f(y) - \varepsilon = \sup\{ f^z_{g_\varepsilon}(t) : \ t \in E_\varepsilon(t)\}$, $y \in E_{\varepsilon'}(x)$.

$$\begin{aligned}
&\Gamma_{\varepsilon'}\Gamma_\varepsilon f(x) + \varepsilon' + \varepsilon \\
&\quad = \sup\Big\{\sup\{ f^z_{g_\varepsilon}(t) : t \in E_\varepsilon(y)\} + \hat{g}^x_{\varepsilon'}(y) : y \in E_{\varepsilon'}(x)\Big\} \\
&\quad = \sup\Big\{ f(t) + \sup\big\{\hat{g}^y_\varepsilon(t) + \hat{g}^x_{\varepsilon'}(y) : y \in E_{\varepsilon'}(x)\big\} \ : t \in E_\varepsilon(y)\Big\} \\
&\quad = \sup\big\{f(t) + \hat{g}^x_{\varepsilon'+\varepsilon}(t) : t \in E_\varepsilon(y)\big\} \\
&\quad = \Gamma_{\varepsilon'+\varepsilon} f(x) + (\varepsilon' + \varepsilon) .
\end{aligned}$$

Therefore $\Gamma_{\varepsilon'}\Gamma_\varepsilon f(x) = \Gamma_{\varepsilon'+\varepsilon} f(x)\ \forall\, x \in X$.

With the now standing dilation operator properties on L^∞_{loc} and the restricted upper semi–continuous functions of $\mathcal{U}$ a new set of functions can be derived. This class functions is called the restricted lower semi–continuous functions of $\mathcal{L}$. The generation of this dual function class is now introduced by the function transform operation of erosion, defined from the operation of dilation.

2.2.19 Definition : If $f \geq 0$, $f \in L^\infty_{loc}$ then $-f \in L^\infty_{loc}$, and the operation of **erosion** is : $\dot{\Gamma}_\varepsilon f(x) = -\Gamma_\varepsilon(-f)(x)$. (3)

The operation of erosion is dual to that of dilation and introduces many additional possibilities for morphological data analysis.

2.2.20 Proposition : If $f \geq 0$, $f \in L^\infty_{loc}$ then $\dot{\Gamma}_\varepsilon f \in \mathcal{L}\ \forall\ \varepsilon > 0$.

proof. Suppose $f \in L^\infty_{loc}$, then $-f \in L^\infty_{loc}$ and
$\Gamma_\varepsilon(-f) \in \mathcal{U}\ \forall\ \varepsilon > 0$.
Therefore, $A^a\Gamma_\varepsilon(-f)$ is open and $C^a\Gamma_\varepsilon(-f)$ is closed . Reversing polarity again then shows $\{x \in X : -\Gamma_\varepsilon(-f)(x) > -a\}$ is open and $\dot{\Gamma}_\varepsilon f \in \mathcal{L}$.

Since dilation and erosion are duals, each property of dilation also has a dual property with erosion, which can be proved with this duality principle, hence proofs will be omitted.

2.2.21 Definition : If $f \in \tilde{\mathcal{L}}$, $f \geq 0$, $\lim_{\varepsilon \to 0} \dot{\Gamma}_\varepsilon f = f \in \tilde{\mathcal{L}}$.

2.2.22 proposition :

i) $\dot{\Gamma}_\varepsilon f \leq \dot{\Gamma}_{\varepsilon'} f$ if $\varepsilon \geq \varepsilon'$.

ii) $\dot{\Gamma}_\varepsilon f(x)$ is continuous with respect to ε, $\forall\ \varepsilon > 0$, $x \in X$.

2.2.23 proposition : given the erosion mappings $\dot{\Gamma}_\varepsilon$, $\dot{\Gamma}_{\varepsilon'}$, constructed with the convex structuring element g, the composition map has the property :

$$\dot{\Gamma}_{\varepsilon'}\dot{\Gamma}_\varepsilon f = \dot{\Gamma}_{\varepsilon'+\varepsilon} f \quad \forall f \in L^{\infty}_{inc} . \tag{4}$$

If the finite values of X and g are binary valued these definitions of erosion and dilation correspond to their binary counterparts.

With the operations of dilation and erosion the less destructive operations of opening and closing may be performed. These operations of closing and opening conform, respectively, to the definitions of maximum enclosure and minimum cover of a data mapping for unions of the structuring element as it is translated. Opening is of particular importance in the development of the morphological skeleton, a minimal image representation, which is defined from deviations of the image from the shape of the structuring element across a spectrum of scales.

2.2.24 Definition : fuzzy opening, (5)

$f_{\varepsilon g} = \Gamma_\varepsilon \dot{\Gamma}_\varepsilon f$, g is precompact − convex, $\varepsilon > 0$.

properties : anti–extensive $f_{\varepsilon g} \subset f$,

idempotent $(f_{\varepsilon g})_{\varepsilon g} = f_{\varepsilon g}$,

increasing $f \subset h \Rightarrow f_{\varepsilon g} \subset h_{\varepsilon g}$.

2.2.25 Definition : fuzzy closing, (6)

$f^{\varepsilon g} = \dot{\Gamma}_\varepsilon \Gamma_\varepsilon f$, g is precompact − convex, $\varepsilon > 0$.

properties : extensive $f^{\varepsilon g} \supset f$,

idempotent $(f^{\varepsilon g})^{\varepsilon g} = f^{\varepsilon g}$,

increasing $f \subset h \Rightarrow f^{\varepsilon g} \subset h^{\varepsilon g}$.

The structuring elements of this paper are limited to arbitrary transpose invariant convex shapes which are selected to measure the size or orientations of image features as erosion and dilations are successively cascaded. An interesting property of dilation and erosion is that a homogeneous succession of these respective operations is equivalent to one operation with the composite dilation of the entire group of structuring elements, eq. (2), (4). Thus the minimum diameter of a convex object is derived by a succession of erosions with a spherical structuring element until the object representation is deleted. Likewise the maximum diameter of a convex object may be ascertained with a succession of dilations with the same spherical structuring element.

Implementation of morphological opening operations for diametric analysis has clearly provided a segmentation tool for the unobscured visualization of intracranial anatomy and internal organs from X–ray CT and magnetic resonance imagery [13, 14, 15]. In particular neurological surface anatomy is segmented from 3–D acquisitions due to properties of size and convexity across a spectrum of scales relative to the concave 2–D surface features of the enveloping extracranial tissues (Figure 3). For grayscale morphology, convexity also extends to the graylevels of the image data and thus requires that the features of the segmented object be the brightest or darkest within some scale of interest. Since erosion and dilation or opening

and closing are related by set complementation it is equally possible to segment dark features by use of dilation and closing operations. This property is exploited to segment the ventricular system of the brain (Figure 9). For MRA studies the surface stripping properties of 3–D erosion is also exploited to eliminate extracranial capillaries for unobscured visualization of the intracranial arterial and venous tree. Unfortunately, most applications of mathematical morphology, unlike the methods introduced in this paper, do not extend beyond this level of morphological processing and hence destroy most of the high resolution detail of the segmented objects.

2.3 Morphological Skeleton

The representation of non–convex or concave topological characteristics, such as curvilinear features, over a spectrum of neighborhood scales is supported in mathematical morphology by a skeletonization technique. The morphological skeleton representation of an image is developed by the collection of successive shape deviations of an image set from a structuring element across a spectrum of scales. For arteries and veins this maps a uniform diametric representation when the circular structuring element is used.

It is apparent from the examples that morphological opening and closing operations destroy features, within an image, which deviate from the shape, size or orientation of the structuring element. To preserve these complementary features the morphological skeleton is used. Thus image features which deviate from the properties of size, shape and orientation of the structuring element are preserved within the morphological skeleton. The construction of the morphological skeleton of an image proceeds by differencing successively larger scales of morphological erosions until the image erodes to a monotone intensity, or successively larger scales of morphological dilations of an image from a largest scale, which just dilates the image to a monotone intensity.

Thus maximal features within a neighborhood scale (white) as well as minimal features within a neighborhood scale (black) are represented within the morphological skeleton.

To represent the white skeleton the anti–extensive operations of erosion and opening are performed.

2.3.1 **Definition :** $S^{\epsilon}_{\alpha}(g, f) = (\dot{\Gamma}_{\alpha} f) \setminus (\dot{\Gamma}_{\alpha} f)_{\alpha\epsilon}$. (7)

$$d = \underset{\alpha \in \Re^{+}}{\liminf} \{\alpha : \inf(f_{\alpha\epsilon}) = \sup(f_{\alpha\epsilon})\} .$$

$$S^{\epsilon}(g,f) = \sum_{0 \le i \le l+d} S^{\epsilon}_{i}(g, f) , \quad \text{is the white skeleton.}$$

Alternately for a black skeleton the extensive operations of dilation and closing are performed.

2.3.2 **Definition :** $S^{\epsilon}_{-\alpha}(g, f) = (\Gamma_{\alpha} f)^{\alpha\epsilon} \setminus (\Gamma_{\alpha} f)$. (8)

$$b = \underset{\alpha \in \Re^{+}}{\liminf} \{\alpha : \inf(f^{\alpha\epsilon}) = \sup(f^{\alpha\epsilon})\},$$

For digital raster formats of pixels or voxels ϵ is equal to 1.

$S^s(g, f) = \sum_{0 \le i \le 1+b/s} S^s_{-i}(g, f)$, is the black skeleton.

2.3.3 **Definition :** $S^s(g, f) = \sum_{-1-b/s \le i \le 1-a/s} S^s_i(g, f)$, (9)

the total skeleton.

An important feature of the skeleton is that the original image may be reconstructed without precision loss with dilations and additions of the positive morphological skeleton components $S_\alpha(X)$ or with erosions and additions of of the negative skeleton components $S_{-\alpha}(X)$. For grayscale images these equations are expressed in a recursive form :

2.3.4 **Definition :** $f_{ws} = \Gamma_g f_{(p+s)g} + S^s_p(g, f)$, $f = f_{0-g}$. (10)

white skeletonal reconstruction.

Likewise to represent closings of the image the negative components of the skeleton are used.

2.3.5 **Definition :** $f^{bs} = \Gamma_g f^{p+sg} - S^s_{-p}(g, f)$, $f = f^{0-g}$. (11)

black skeletonal reconstruction.

2.4 Fuzzy Connectivity

Connectivity is a characteristic of the morphological skeleton preserved relative to the corresponding image structures if a convex structuring element with finite surface curvatures is selected. The capacity of the morphological skeleton to preserve the connectivity of image structures is exploited by the algorithms of this paper. For digital imagery and fuzzy sets the actual definition of continuity, however, must be defined. The continuity of a skeleton representation is defined relative to the structuring elements used to make the morphological skeleton. To facilitate this definition the introduction of a modified Hausdorff metric provides the means of measuring the connectivity of image structures. The Hausdorff metric was devised to measure the distance and dissimilarity of sets, a nonlinear set analog to inner product correlation. This metric is precisely defined by mathematical morphology if a circular structuring element is utilized. A modified metric may likewise be devised with variously shaped structuring elements of relative convex and symmetric characteristics, Proposition 2.2.10. This metric likewise generalizes to a metric distance between functions with proposition 2.2.11.

modified Hausdorff metric between functional maps f and h in restricted $\mathcal{U}$, ,

2.4.1 **Definition :** Modified Hausdorff function metric (12)

$$d_g(f, h) = \inf\{\alpha : \sup(f \wedge h) \le \inf(\Gamma_\alpha f \wedge \Gamma_\alpha h)\} .$$

if f is connected by distance $\varepsilon > 0$, and element g then $d_g(f(x), f(y)) \le \varepsilon$ for all points $x, y \in X$.

For the 3–D digital image applications of this paper connectivity is limited to a unity radial scale of the 3x3x3 basis structuring elements relative to the Hausdorff metric.

2.4.2 **Proposition :**

if an image f is distance ε and element g connected then :

$$S_0(g, f) = f - f_{\varepsilon g}, \; f_{\varepsilon g} \subset f, \tag{13}$$

proof. $S_0(g, f)$, $f_{\varepsilon g}$, are distance ε and element g connected, by definition 2.3.1. Likewise $S_\varepsilon(g, f)$, $(\Gamma_\varepsilon f)_{\varepsilon g}$ are distance ε and element g connected. (14)

This proposition is exploited in morphological reconstruction techniques based on fuzzy connectivity.

The morphological skeleton is also a reduced representation of the image, since due to properties of opening no set interiors exist, which is ideal for image compression [18], and analysis of multiscale curvilinear features of images, independently from diametric features. For 3–D data sets the morphological skeleton consists of forms which are immeasurable to a 3–D structuring element such as 2–D surfaces, 1–D curves and 0–D point noise. For curvilinear feature segmentation the morphological skeleton is an ideal representation since arteries and veins are represented as 1+D curvilinear forms with uniform diameters of thickness immeasurable to the scales of the structuring element used. This is due to the dimensional filtering characteristic of opening since features of lesser dimensional measure are consistently covered by collections of structuring elements of larger euclidian dimensionality and thus filtered (Figure 5) and placed into the morphological skeleton. The ability of the morphological skeleton to represent features over a range of neighborhood scales and within a range of integer dimensional bounds permits the representation of fractal features or fractional dimension, which is demonstrated in the results section.

2.5 Segmentation of 3–D Features Based on Fuzzy Connectivity

Intracranial features of the brain are segmented from MRI acquisition based upon a morphological size filter of their large extent followed by a morphological reconstruction based upon fuzzy connectivity of smaller scale features from the grayscale skeleton components. This provides the restoration of the high resolution features, particularly brain surface and arterial features. The size filter is based upon cascaded erosions, eq. (4), with a spherical structuring element, Figure 2, until the extracranial tissues are deleted due to the lack of convexity and diametric properties of the scaled structuring element. Coincidentally, the spectral components of the skeleton can be formed from the difference of the openings of the successive erosions of the image, eq. (7), for algorithm optimization. The morphological reconstruction of the high resolution 3–D data features proceeds by selectively adding connected skeletal component features in an interative process from large to small scale based on connectivity with the modified Hausdorff metric, eq. (12). Fundamentally the skeletal features are added to the reconstruction based upon principals of fuzzy set connectivity proposition 2.4.2 [14, 15]. Additional requirements of the morphological skeleton relative to 1+D curvilinear features are addressed in the following methods section of this paper. The fundamental principal of segmenting image structures based on size and connectivity is demonstrated in Figure 3 and Figure 12.

2.5.1 **Definition :** Morphological reconstruction based upon fuzzy connectivity ,

$$R^{\tau}_{d}(f) = (\Gamma_{\tau} R^{\tau}_{d}(f)) + [S^{\tau}_{d}(g, f) \wedge (\Gamma_{\tau} R^{\tau}_{d+\tau}(f))] \quad (15)$$

$R^{\tau}_{d \le d}(f) = f_{d_{\infty}} = S^{\tau}_{d}(g, f) = \emptyset$. .

$d = n\varepsilon < d + \varepsilon$, $n \in N$. for digital images ε is 1.

$R^{\tau}_{0}(f)$ is the completed reconstruction.

2.6 Morphological Scale Spectra of Skeleton Components

A similarity of the morphological set analysis to Fourier analysis is the ability to represent image data with spectral distributions. The frequency content of the morphological spectrum are however relative to tractable shapes rather than the more abstruse representation of frequency for sinusoidal function spectra in the Fourier distribution. The idea of the shape spectra of images was developed by Matheron [20] to define probabilistic size distributions of shapes for the study of 2–D binary sets on continuous domains. Serra furthermore applied this technique to study the porosity of petrographic and biological images [22, 23]. The development of a morphological frequency spectrum is based upon the measures of the components of the morphological skeleton. The frequency magnitude (PS_{α}) of each spectral point (α) of scale or orientation is therefore related to the volume measure of the morphological skeleton components.

2.6.1 **Definition :**

White spectral distribution,

$$PS_{\alpha}(g, f) = \frac{d}{d\alpha} |\Gamma_{\alpha} f|_1 = \lim_{\varepsilon \downarrow 0} \frac{1}{\varepsilon}[|\Gamma_{\alpha} f|_1 - |\Gamma_{\alpha+\varepsilon} f|_1] . \quad (16)$$

Black spectral distribution,

$$PS_{-\alpha}(g, f) = \frac{d}{d\alpha} |\Gamma_{\alpha} f|_1 = \lim_{\varepsilon \downarrow 0} \frac{1}{\varepsilon}[|\Gamma_{\alpha+\varepsilon} f|_1 - |\Gamma_{\alpha} f|_1] . \quad (17)$$

$|\cdot|_1$ denotes the Lebesque measure on X, $|f|_1 = \int_X f \, dm$.

For digital raster formats of pixels or voxels, α is limited to the integer domain Z and ε is equal to 1. The spectral distribution of shape for digital images is furthermore approximated with the volume of the morphological skeleton, represented as the sum of grayscale integer voxels intensities :

2.6.2 **Definition :** Spectral distributions for digital data,

$$PS_{\alpha}(g, f) = |\Gamma_{\alpha} f|_1 - |\Gamma_{\alpha+1} f|_1 , \quad \text{white} , \quad (18)$$

$$PS_{-\alpha}(g, f) = |\Gamma_{\alpha+1} f|_1 - |\Gamma_1 f|_1 , \quad \text{black} . \quad (19)$$

For Figures 3 and 4 the pattern spectra analysis of this continuous binary model of a MRI transverse section, through the brain, is exemplified qualitatively without high resolution features in Figure 6 for infinitesimal dilations and erosions. Presented in this spectral dis-

tribution is a positive spectral component where the encircling extra–cranial ring disappears due to erosion at a spectral scale and a negative spectral component where the dark ring representation of the skull disappears due to dilation at a negative spectral scale. For biomedical image acquisitions or synthetic aperture radar (SAR) clutter data with rich morphological content the behavior these scale spectral distributions relate a description of the more complex and fractal nature of biological structures, particularly for the neurological and the vascular systems. The preservation of this nature is an extremely important attribute in the visual representation and human evaluation of biomedical imagery.

A more general interpretation of the spectral distribution is related to the Minkowski content δ_{μ}, which can be generalized to functions over an image domain with the structuring element base $\mathfrak{B}_g$. The result provides a means of measuring fractal dimension, s, however in a more restricted sense than the Hausdorff dimension. (i.e. find s such that log μ is bounded)

2.6.3 Definition : Minkowski Content μ is a scalar function mapping dependent on $s \in [0, n]$ of $f \in L^{\infty}_{bc}$,
white lower bound,

$$\lim_{\varepsilon \downarrow 0} \frac{\|\check{f}\|_1 - \|\Gamma_\varepsilon f\|_1}{\varepsilon^{n-s}} = \mu_-(s) \; . \; \lim_{\varepsilon \downarrow 0} \Gamma_\varepsilon f = \check{f} \in \check{\mathcal{L}} \; . \quad (20)$$

black upper bound.

$$\lim_{\varepsilon \downarrow 0} \frac{\|\Gamma_\varepsilon f\|_1 - \|\hat{f}\|_1}{\varepsilon^{n-s}} = \mu_+(s) \; . \; \lim_{\varepsilon \downarrow 0} \Gamma_\varepsilon f = \hat{f} \in \hat{\mathcal{U}} \; . \quad (21)$$

2.7 Size Filtering with Morphological Scale Spectra and Skeleton Components

A further similarity of the morphological size spectral distributions to the Fourier transform is the ability to perform frequency filtering of the spectral components. Hence it is possible to perform bandpass, band–reject, highpass or lowpass filtering of the shape size composition of an image. In this manner a spectral filter F(α) may be defined over the size spectral domain. Specifically size filtering introduces a new postprocessing methodology for segmenting static tissues from MRA acquisitions.

For the 3–D MRI images the discriminating feature of static tissues of the brain is a convexity property across a broad range of neighborhood scales relative to the limited radius of intracranial arteries and veins. Filtering this convexity feature over a broad range of scales permits the selective elimination of static tissues by limiting the scale of morphological reconstruction to within the radius of arteries and veins. In effect this technique is a selective feature scale filtering and enhancement technique. To perform this preprocessing operation a size spectral filter is defined.

2.7.1 Definition : $F(\alpha) = 1$ for $0 \leq \alpha \leqq v$, and $F(\alpha) = 0$ $v \leq \alpha$.

i.e. Morphological reconstruction based upon a limited range of diametric scale v, v is the approximate maximum diameter of arteries and veins.

With this scale filter the convexity properties of images over a pattern spectrum are selectively enhancement or suppression to assist visualization and image analysis.

2.7.2 Definition :

$$f_{\alpha_0}^{\sim} = \Gamma_\varepsilon f_{(\alpha+\varepsilon)_0}^{\bullet} + F_\nu(\alpha) S_\alpha(g, f)$$

$$\text{where } S_\alpha^{\bullet}(g, f) = F(\alpha) S_\alpha(g, f) = \sum_{\alpha \le \nu} F(\alpha) S_\alpha(g, f) . \qquad (22)$$

$f^{\sim} = f_{\alpha_0}^{\sim}$, is the limited scale reconstruction.

2.8 Curvilinear Feature Segmentation

The curvilinear features of images are discriminated and enhanced from other concave features, such as surfaces and noise, due to their behavior relative to 1–D structuring elements. This analysis exploits maximum comparison, by opening, and minimal comparison, by closing, of 1–D line segments oriented, at various angles and scales of length [17, 18]. The morphological skeleton representation of the image is used due to the reduced dimensional representation of curvilinear forms of the arteries and veins as 1+D curves of uniform diameter. In particular a hierarchical representation by cascading maximum orientations extends the scale of interest for selection of arterio–venous curvatures. This technique may likewise be extended to analyze 2–D surface features with 2–D planar shaped structuring elements at various angles of orientation. This capability of dimensional form filtering extends to a broader application for the operation of erosion, and complimentarily the operation of dilation, a capability of analyzing dimensional forms and representing data features in the skeleton of a hence lesser dimensional form to that of the structuring element. Such as for a spherical structuring element the skeleton contains points, curves, surfaces. Figure 5 lists a chart of the discriminated forms based of the structuring element dimensionality.

Curvilinear analysis differs from the size and convexity analysis of the preceding segmentation schemes primarily due to the reduced dimensionality of the structuring element from 3–D sphere to a 1–D segment and hence the greater sensitivity to the orientations of curvilinear structures (Figure 8). Erosion with this structuring element eliminates impulse noise as well as curve and surfaces points which do not have parallel tangents to the segment. Utilizing the supremum over all orientations of opening with the 1–D structuring element filters noise and define the appropriate tangent direction of curvilinear features eq. (23). The infimum over all orientations of closings with the 1–D structuring element defines the tangent direction, Figure 7, and enhance the curvilinear features of the MRA acquisitions, eq. (23). The length of the 1–D structuring element is also scaled for improved sensitivity to the curvatures of curvilinear forms, Figure 8.

2.8.1 Definition : The median operations are :

$$\text{erosion, } \Gamma_t^{\kappa} f = \bigvee_{\omega \in \Omega} \Gamma_t^{\ell(\omega)} f , \quad \text{dilation, } \dot{\Gamma}_t^{\ell} f = \bigwedge_{\omega \in \Omega} \dot{\Gamma}_t^{\ell(\omega)} f .$$

$$\text{opening, } f_{t\ell} = \bigvee_{\omega \in \Omega} f_{t\,\ell(\omega)} , \quad \text{closing, } f^{\kappa} = \bigwedge_{\omega \in \Omega} f^{\kappa(\omega)} . \qquad (23)$$

$\ell(\omega)$ – denotes the 1 – D oriented structuring element at solid angular ω within the domain Ω.

$\wedge$ denotes an infimum over X of a collection of functions .

$\vee$ denotes an supremum over X of a collection of functions .

Equations of (23) describe modified median filter operations.

for digital imagery:

ℓ_i– denotes the 1–D structuring element at orientation i,
$i \in \{0,\ldots,12\}$, denotes the 13 possible digital orientations of a 3–voxel segment within a 3x3x3 voxel matrix.

Curvilinear or reduced dimensional analysis further offers a means of morphological skeletonization over a range of scales, relative to the lengths of the variously oriented structuring elements. The analysis of this skeleton demonstrates curvature information about the curvilinear forms of veins and arteries. Intuitively, this analysis is reasonable since smaller curvatures, as apposed to larger, should be less sensitive to changes in the scale length of the 1–D structuring element. For digital imagery curvilinear forms have the finite dimensions of voxels which permits curvilinear analysis over a broad range of scales.

2.8.2 **Definition :** Oriented skeleton ,

$$S_i^{\ell}(\ell, f) = \left(\Gamma_i^{\ell} f\right) \setminus \left(\Gamma_i^{\ell} f\right)_{\varepsilon\ell} , \tag{24}$$

$$S_{-i}^{\ell}(\ell, f) = -\left(\Gamma_i^{\ell} f\right)^{\varepsilon\ell} \setminus \left(\Gamma_i^{\ell} f\right) . \tag{25}$$

Curvilinear analysis is only performed upon the morphological skeleton, formed from eq. (7) which exclusively contains < 3–D dimensional forms. This restriction upon curvilinear analysis is imposed since the varying diameters of arteries and veins as well as static tissues of the brain, in the original MRA data set, are 3–D forms which are invariant to the oriented 1–D structuring elements used for curvilinear analysis (Figure 5).

Hence the curvilinear reconstruction is based upon a limited scale of the morphological skeleton to eliminate static tissues from the image. The connectivity criteria is also used to eliminate extracranial tissue features of the morphological skeleton for an analysis focused upon 1–D curvilinear features. An enhancement of the composite skeleton is thus possible with a technique, eq. (26) similar to the intracranial reconstruction process, eq. (15).

2.8.3 **Definition :**

$$CL1_i^{\ell}(\ell, S^{\varepsilon}) = \left[\Gamma_i^{\ell} CL1_{i+1}^{\ell}(\ell, S^{\varepsilon})\right] + S_i^{\ell}(\ell, S^{\varepsilon}) \wedge \left[\Gamma_i^{\ell} CL1_{i+1}^{\ell}(\ell, S^{\varepsilon})\right] , \tag{26}$$

$$CL1_i^{\ell}(\ell, S^{\varepsilon}) = \emptyset, \quad r \geq r .$$

Further enhancement can be provides with median closing,

$$CL1_i^{\ell}(\ell, S^{\varepsilon}) = \bigvee_{0 \leq r \leq r} \left(\left[CL1_i^{\ell}(\ell, S^{\varepsilon})\right]\right)^{r\ell} \tag{27}$$

For 3–D digital MRA studies equation (26) requires $r = 2$ to approximate arterio–venous curvatures and $\varepsilon = 1$ voxel spacing. A simpler approach is to perform only one opening and one closing operation on the skeleton for filtering and enhancement respectively. This approach however does not preserve image features well when r becomes larger due to the lack of a connectivity criteria.

$S \equiv S^{\circ}(g, f)$, is th composite skeleton of the image
f derived with a spherical structuring element, g,
of diametric scale $\leq$ the maximum diameter of arteries and veins.

2.8.4 Definition :

$$CL2(\ell, S^{\circ}) = S^{\circ} \wedge (S^{\circ}_{\ell})^{rf}, \text{ where } S^{\circ} \equiv S^{\circ}(g, f) . \quad (28)$$

Equation (27) yields noise suppression and enhancement of the limited scale morphological skeleton, typically $r = 1$ or 2 for 3–D digital MRA studies. In general to retrieve the true diametric representation of the arteries and veins the results of equations (26, 27) are used to reconstruct a filtered representation of the image.

2.8.5 Definition :

$$R^{\circ}_{r}(f) = \left[\Gamma^{\circ}_{1} R^{\circ}_{r+1}(f) \right] + S^{\circ}_{r} \wedge CLn(\ell, S^{\circ}) , \; S^{\circ}_{r} \equiv S^{\circ}_{r} (g, f) . \quad (29)$$

$R^{\circ}_{0}(f)$ is the limited scale reconstruction for $r = 0$.

3.0 Results

Grayscale morphological analysis of a spin proton image section through the brain was used to illustrate the elementary aspects of morphological description. In Figure 10 an example of segmenting the intracranial brain tissue from the extracranial tissues of the scalp is presented, Figure 10c in comparison with Figure 10b. The method utilized is similar to the idealized version shown in Figure 3, however, the fuzzy connectivity reconstruction technique, eq. (15), was used to restore small scale morphological features of the brain after size filtering. This same technique was extended to 3 dimensions to segment intracranial features for unobscured surface visualization of the brain, Figure 12.

To demonstrate a morphological skeleton and its behavior the skeletal components S_{α} of the image were derived with eq. (7) up to the maximum diameter d which eroded the image to a monotone value. Two 3x3 pixel structuring elements were used in a cascaded succession of erosions to generate the spectrum of necessary scales, eq. (4). The shapes of the structuring elements were selected to approximate a circle, one of a diamond shape and the other of an octagonal shape. It should be emphasized that the reconstruction of the image from its morphological skeleton components, eq. (10), is lossless relative to the original image. The sum of these skeletal components, eq. (8), are visible in Figure 10a. This Figure illustrates a 1–D curvilinear form of the composite skeleton which is a reduced representation of the 2–D morphology of the imaged brain section. Furthermore the integral volume of the skeletal components eq. (18), over a spectrum of diameters produces a size spectral distribution, Figure 11, which demonstrates a Hausdorff or fractional dimension of the brain section relative to a logarithmic scale. In particular the first slope over a range of the smallest structuring element diameters indicates a 1.65 Hausdorff dimension which is basic to the morphology the brain gyri represented in this 2–D section. By selecting a particular set of "bones", Figure 10d, from the skeleton it is possible to independently reconstruct the image features of the bones, Figure 10e, or to see the image with the features of the bones missing, Figure 10f. This example particularly represents the natural and fuzzy representation of image features with grayscale morphology. The technique introduced for the analysis of the morphological

skeleton of MRA acquisitions, eq. (26, 27, 28), provides a means of selecting these skeleton bones based features of one dimensional curvilinear forms. These broad capabilities of the morphological skeleton to represent imagery without distortion, preserve connectivity, isolate diametric features, and to furthermore represent the natural or fractal nature of imagery posed the morphological skeleton as an ideal and extremely attractive representation for arteries and veins, from MRA acquisitions.

Figure 13 demonstrates a magnetic resonance angiography study of the carotid arteries of the neck. The arteries are selected relative to flow velocity directions toward the extremity of the head from the body. An undesirable artifact from this imaging technique is that arterial flow oblique to the selected flow direction is distorted resulting in a staircase effect. The objective with this study is to enhance the arteries within the 3–D volume of the data. The unadulterated data is initially observed with a transparency projection algorithm, performed through a succession of projection angles. The first method to exploit the curvilinear features of arteries and veins is to represent arterio–venous features in a uniform diametric representation. This representation is rendered by the morphological skeletonization of arteries and veins which defines a central axis of the arteries i.e.. Figure 13b. The arteries of the skeleton representation are approximately of a single voxel diametric width to simplify curvilinear analysis of the arterio–venous features. This single voxel representation allows features of curvature and length to be analyzed independent of the diametric scale of the artery or vein. The limited scale morphological reconstruction, eq. (22), was used to enhance this study by eliminating static tissue over a broad range of scales followed by application of eq. (26, 28) to eliminate capillary features, Figure 14c versus Figure 14f. Of particular importance it the fact that the diameters of the arteries and veins are unchanged by this scale selective technique. Additionally, the "stair case" artifact has been eliminated from the oblique flow arterial acquisitions.

The visualizations of Figure 14 were acquired at a courser resolution than Figure 13, however these scans encompass the broader range of the carotid arterial tree which feeds the base of the brain. The basal arterial features of the brain were enhanced, in Figure 14a, by the elimination of posterior and anterior coronal slices for a region of interest (ROI) study. To eliminate the expert intensive and computer interactive techniques of ROI selection, the automated methods of this paper can be used to eliminate extracranial and subdural capillaries for unobscured visualization of arterial tree. Once again eq. (22) is eliminates image features of diametric dimensions larger than the arteries and veins, thus only a limited scale morphological skeleton reconstruction was used. Curvilinear segmentation of the limited scale morphological skeleton with eq. (26, 27) then eliminates 0–D point noise and limits arterial curvatures with line segments of various lengths and orientations. Thus segments of 3 and 5 voxels in length, or radius, $r = 1$ and 2, were used with maximum values of orientation in 13 directions, eq. (23). This segmented skeleton then provides a basis to morphologically reconstruct the enhanced data volume for reprojection and visualization. Figures 14b and 14e show examples of the filtered morphological skeleton axinometrically projected along 2 different angles of direction. Figures 14c and 14f are the projections of the filtered MRA volume. Note the preservation of small diametric features between projections of the original volume 11a and the filtered volume 11c, and note the radical elimination of the obscuring capillaries from Figure 14d demonstrated in Figure 14f.

Figure 15 demonstrates a study for visualizing the arteries and veins of the head. Again a directional flow field was selected to enhance blood flows through the transverse plane to-

wards the superior of the head. Since arteries and veins have no particular direction in the head both types of flow are realized by this imaging method. The elimination of extracranial veins as well as capillaries is the objective for this study, particularly since intracranial arteries and veins are of paramount importance for planning neurological surgeries. To facilitate this objective, eq. (15) has shown the capability of segmenting intracranial features for unobscured 3–D visualization of the brain, Figure 12, and now may be used to include the segmentation arteries and veins within the proximity of the static brain tissues. Figures 15a and 15b demonstrate two projected directions of the MRA study, extracranial capillaries obscure the visualization of the intracranial arteries and veins and must be eliminated. Equation (15) was used to segment the static tissues of the brain based upon a size and connectivity criteria, which permitted the unobscured visualization of brain anatomy, Figure 14, Figure 15e,f. The static tissue representation defined with this method was then used to mask the intracranial arteries and veins for further curvilinear enhancement eq. (15) and limited scale filtering eq. (22), and eq. (26, 27) which resulted in Figure 12c,d. Comparing Figure 15a,b with Figure 15c,d. we observe that the intracranial arteries and veins are segmented successfully without the overlying extracranial feanures.

In Figure 16 a complex scene is analyzed consisting of foliated trees, tree stump, road and telephone poles. The original image is demonstrated in the upper left. In the upper left a 2–D structuring element is used, operator g in eq. 21, to develop a morphological skeleton, and then reconstruct the image based on fuzzy connectivity of the skeleton components, eq. 25. note the preservation of foliage details and elimination of manmade features such as the road sign and lane strip on the road. In the lower left a 3x3 median opening operation, consisting of 4 1–D oriented structuring elements, was employed in a succession of 20 cascaded operations [12]. This operation preserved the 1–D features of the image, including man–made features of the sign and lane strip on the road, and eliminated the feanures of leaves from the trees. The leaves have a characteristic dimension less than one in the image and are filtered by the 1–D oriented operations of the median erosion, eq. (23). In the lower right a median dilation, eq. (23), consisting of four 1–D oriented structuring elements, was used on the eroded image to fill the textual features segmented by median erosion. This median operation of erosions followed by dilations results in a more convex representation of image features such as leaves.

In Figure 17, a synthetic aperture radar image is analyzed consisting of several specular targets in a speckle noised clutter background. The original image is demonstrated in the upper left. Successively morphological median dilation operations are used to fill the fractal features of the clutter and leave the impulsive specular details of the man–made targets unaltered [12].

4.0 Conclusion

Mathematical morphology has provided a powerful segmentation tool for the unobscured presentation of 3–D brain anatomy [2, 4] and now can eliminate noise and static tissues for a clear demonstration of the intracranial arterial tree from MRA acquisitions. In particular the fine structures of arteries and veins are preserved by the curvilinear feature segmentation with mathematical morphology.

A theoretical development of a battery of morphological analysis techniques have been developed and applied to biomedical and remote sensing image data. These techniques analyti-

cally capture the dimensionality, fractal nature and fuzzy set structure of features from the image acquisitions. A variety of structuring elements, digitally familiar to spheres, planes, and lines defined over a 3–D domain, have been utilized over a spectrum of scales and orientations to segment features of similar or complementary dimensions and shape. In particular, the complementary dimensional features of fractals are preserved as deviations in the morphological skeleton across a wide range of scales relative to the diameter of the convex structuring elements.

The image analysis of mathematical morphology has demonstrated an ability to segment 3–D biomedical image features of magnetic resonance imagery acquisitions and 2–D natural clutter features from remotely sensed SAR images for an unobscured visualization of features of interest from axinometric sum projections. In comparison with intensity histogram and thresholding techniques the distributions of shape spectra, eq. (16, 17), of data are thresholded and mapped as a new analysis and visualization tool, e.g. eq. (22), just as intensity histograms are thresholded and mapped.

Three progressively improving methods for segmentation of the curvilinear features of arteries and veins from MRA acquisitions were introduced. A successive application of these methods illustrated an evolutionary refinement of algorithms to segment intracranial arteries and veins from MRA studies. One of these methods alternately provided a means of segmenting brain tissues from the involvement of extracranial tissues eq. (15). Alternately, a technique established a means of suppressing static tissue features from MRA projections eq. (22), and enhancing curvilinear features eq. (26, 27, 28). This technique successfully addressed the segmentation requirements of the peculiar curvilinear nature of MRA acquisitions, a resplendent example is the comparison of Figures 14d and 14f, and a testament of its accuracy is exemplified in the preservation and enhancement of delicate curvilinear features, comparison of Figure 14a and 14c.

The premise of imagery as a representation over a Borel field topology in mathematical morphology facilitates the analysis of imagery with fuzzy set algebra and offers a catalyst for further advancement into the field of data interpolation and reprojection. In particular, MRI acquisitions and SAR image data are a representation of natural organisms with a property of self similarity at various scales [9] which is consistent to a fractal description [1]. The utilization of the algebra of mathematical morphology makes possible the direct analysis and segmentation of fractal image features relative to spectral distributions of size and shape from the morphological skeleton, as presented in this paper, eq. (16, 17), Figures 10,11. This capability of fractal representation establishes a basis for the most literal and informative presentation and segmentation of biomedical imagery.

Analysis and Segmentation with Fuzzy Operators for Representation/Visualization

Bibliography

1. M. Barnsley, *Fractals Everywhere*, Academic Press, San Diego (1988).
2. H.E. Cline, "Connectivity algorithms for MR angiography," *Society of Magnetic Resonance In Medicine: 9th Annual Conf.* 1, 61 (1990).
3. J. B. Conway, *A Course in Functional Analysis*, Springer–Verlag, New York (1990).
4. K. S. Denison, "The maximum intensity projection as a segmentation tool," *Society of Magnetic Resonance Imaging* 8, 73 (1990).
5. R.A. Drebin, "Volume rendering," *Computer Graphics* 22, 65 (1988).
6. K. Falconer, *Fractal Geometry : Mathematical Foundations And Applications*, Wiley, New York (1984).
7. G. B. Folland, *Real analysis : modern techniques* and their applications, Wiley, New York (1990)
8. G. Gerig, "Medical imaging and computer vision," *M.DAGM–Symp. Mustererkennung–Informatik Fachberichte* 279, 425–430 (1989).
9. A.L. Goldberger, "Fractal description of nature," *Scientific American* 262, 44–50 (1990).
10. F. Hausdorff, "Dimension und ausseres Mass," *Mathematische Annalen* 79, 157 (1919)
11. X. Hu, et. al., "Volumetric rendering of multimodality, multivariable medical imaging data," *Chapel Hill Workshop on Volume Visualization* 1, 45–50 (1989).
12. W.F. Kraske, "Resolvable Analysis and Synthesis of Synthetic Aperture Radar Imagery," *SPIE Intelligent Robots and Computer Vision 11 : Biol. Neural Nets & 3–D Methods* 1826, 317–323 (1992).
13. W.F. Kraske, "VOXAR 3–D Curvilinear Feature Description of MR Angiographic Acquisitions for Graphic Presentation and Analysis," *Soc. of Mag. Res. In Med. : 9th Ann. Conf.* 1, 59 (1990).
14. W.F. Kraske, "3–D Morphological description and visualization of brain anatomy from magnetic resonance imagery," *Radiological Society of North America* 173, pp. 337 (1990).
15. W.F. Kraske, "Morphological description in 3–D volumetric visualization," *Proc. Chapel Hill Workshop on Volume Visualization* 1, 59 (1989).
16. P. Maragos, "A representation theory for morphological image and signal processing," *IEEE Trans. Pattern Analysis and Machine Intelligence* 11, 586–596 (1989).
17. P. Maragos, "Pattern spectrum and multiscale shape representation," *IEEE Trans. Pattern Analysis and Machine Intelligence* 11, 701–716 (1989).
18. P. Maragos, "Morphological skeleton representation and coding of binary images," *IEEE Trans. Acoustics, Speech, Signal Processing* 34, 1228–1240 (1986).
19. P. M. Margosian, "Statistical segmentation and region growing methods," *Society of Magnetic Resonance Imaging* 8, 73 (1990).
20. G. Matheron, *Random Sets and Integral Geometry*, Wiley & Sons, New York (1975).
21. D.R. Ney, "3–D Volume Visualization in Medicine," *IEEE Computer Graphics and Applications* 10, 24–32 (1990).
22. J. Serra, *Image Analysis and Mathematical Morphology*, Acad. Press, New York (1982).
23. J. Serra R.E. Miles, *Buffon Symposium on Geometrical Probability in biomathematics*, Springer–Verlag, 23, Berlin (1978).
24. L.A. Zadeh, *Fuzzy Sets and their Applications to Cognitive and Decision Processes*, Academic Press, New York (1975).

Analysis and Segmentation with Fuzzy Operators for Representation/Visualization

figure 1

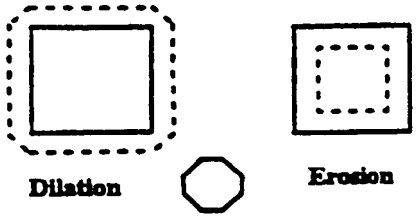

Examples demonstrating dilation and erosion of a square oject relative to the Minkowski addition and subtraction with the given structuring element.

figure 2

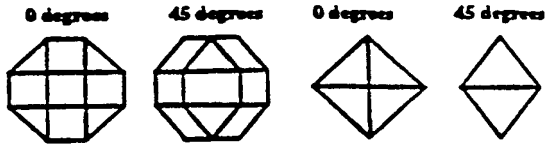

Axinometric projections of the sets used as structuring elements to develop the 3–D grayscale skeletons, a lossless representation of digital imagery. These operators were used alternately to erode and open the 3–D imagery for discrimination of spectral components of the skeleton. Likewise these operators are utilized for morphological reconstruction algorithms.

figure 3

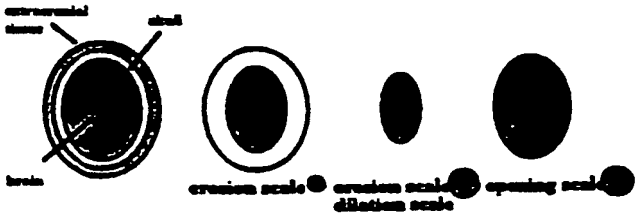

Extra–cranial tissues are deleted due to concavity beyond a particular scale, demonstrated by erosion and opening

figure 4

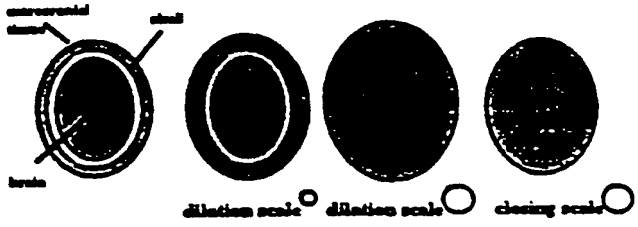

Skull tissues are deleted due to concavity beyond a particular scale, demonstrated by dilation and closing

figure 5

image form

structuring element form	point	curve	surface	volume
point	point	curve	surface	volume
segment	null	curve	surface	volume
disk	null	null	surface	volume
sphere	null	null	null	volume

Filtering of dimensional forms by morphological erosions relative to the structuring element form. The forms filtered to null are complementarily represented in the morph–ological skeleton

figure 6

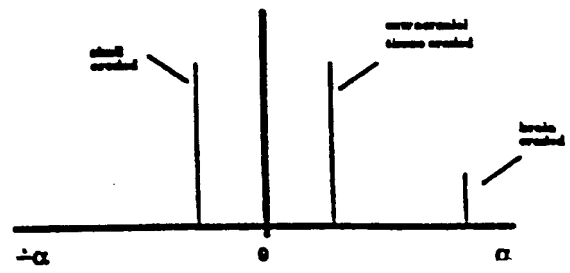

Pattern spectrum of figures 3 and 4
negative spectrum corresponds to dilations of figure 4

Analysis and Segmentation with Fuzzy Operators for Representation/Visualization

figure 7

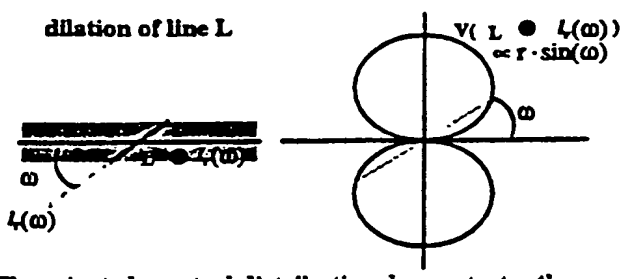

The oriented spectral distribution demonstrates the change in diameter of the line (L) relative to dilations with an oriented structuring element 4(ω)
The line diameter is unchanged with (ω) and L parallel

figure 8

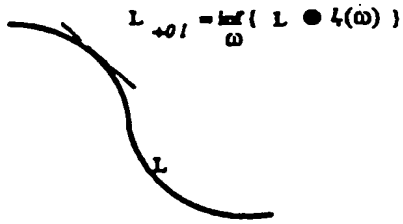

Tangent to curve defined by minimum of oriented spectral distribution at a point of the curve

Sensitivity to structuring element length indicates curvature

Analysis and Segmentation with Fuzzy Operators for Representation/Visualization

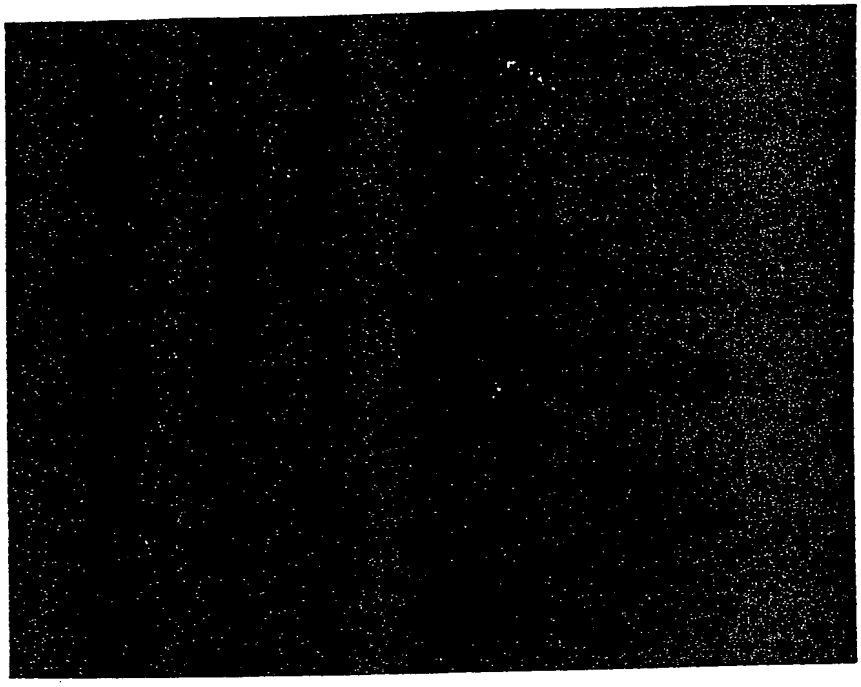

Figure 9 : Ventricles and blood sinuses of the brain. Low contrast ventricular system is demonstrated from overlying subdural cerebral–spinal fluid (CSF) by enhancement of dilation. Blood sinuses, inner brain hematoma, and hemorrhaging superior to the brain are demonstrated by enhancement of erosion.

Analysis and Segmentation with Fuzzy Operators for Representation/Visualization

(a) (b) (c)

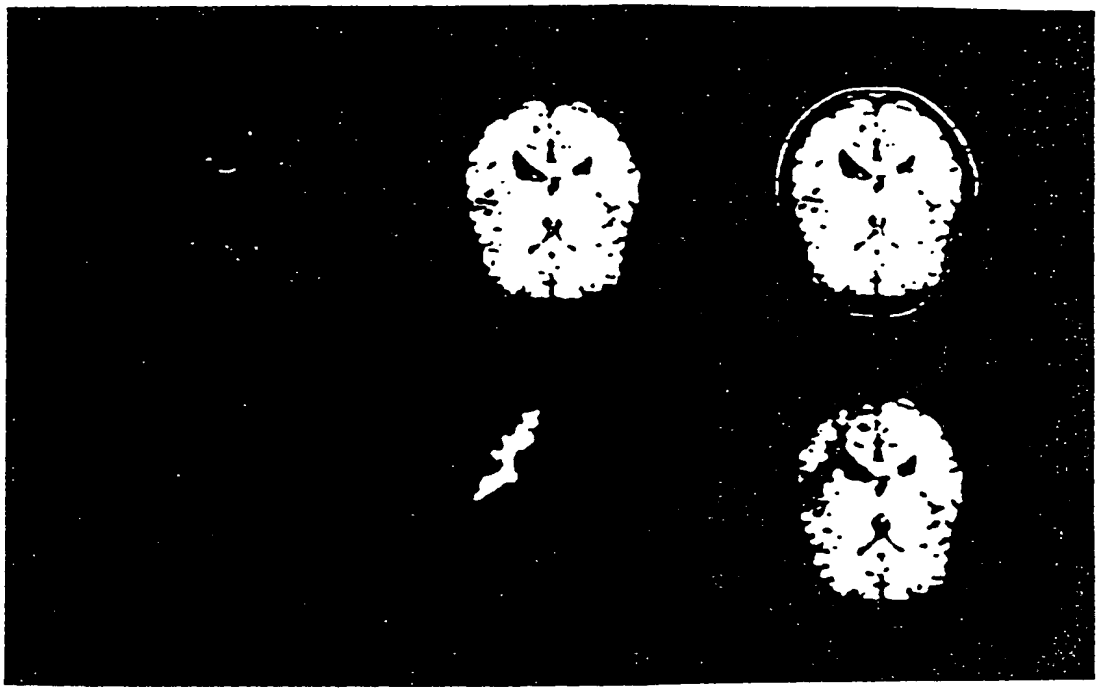

(d) (e) (f)

Figure 10: An array of image processing operations on a proton spin acquisition of a brain section (a) Morphological skeleton with a selected enhancement of a "bone" (b) Segmented neurological tissue (c) Original MRI scan section (d) Selected feature bone of the skeleton (e) Morphologically reconstructed gyri from selected "bone" of skeleton (f) Morphologically reconstructed brain tissue without gyri bone feature from skeleton. Note natural continuity of texture on the boundaries where features are removed.

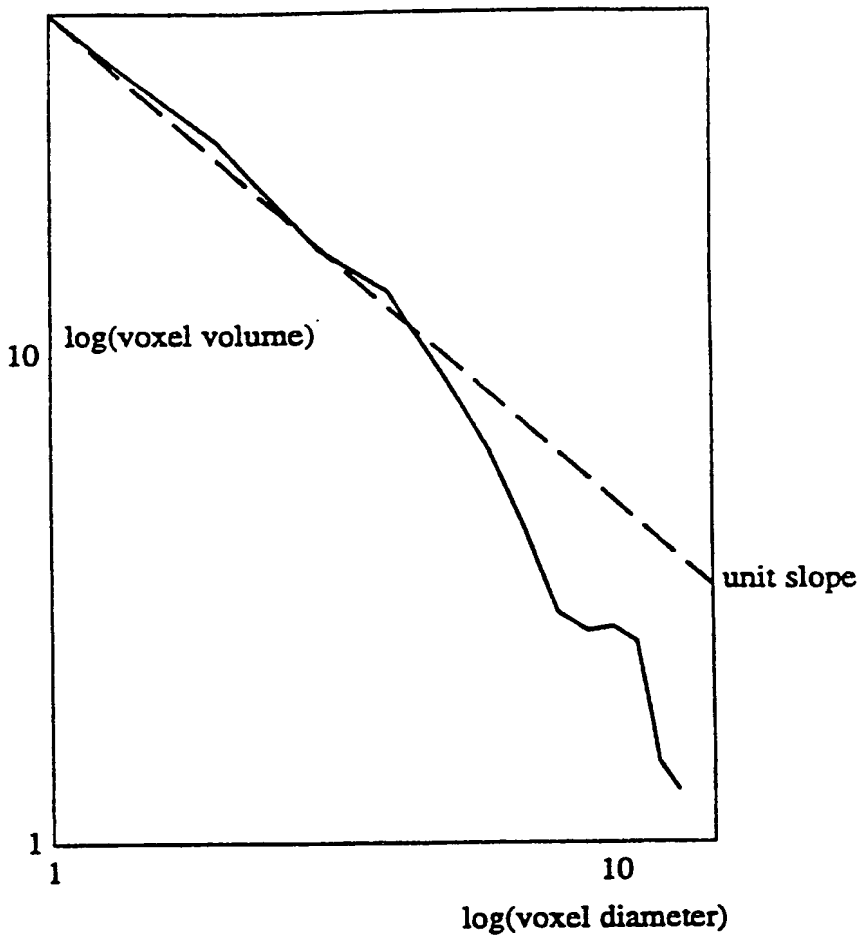

Figure 11 : Log–log distribution of size spectra relative to the volume measure of each spectral component of the morphological skeleton. In the smallest scale region of the distribution the slope corresponds to the fractal dimension of the gyri of the brain scan section of Figure 10. Utilizing the first eight voxel diameters for a least means square quadradic fit estimates the gyri to have an 1.65 dimensional representation within the 2–D scan section.

(a) (b)

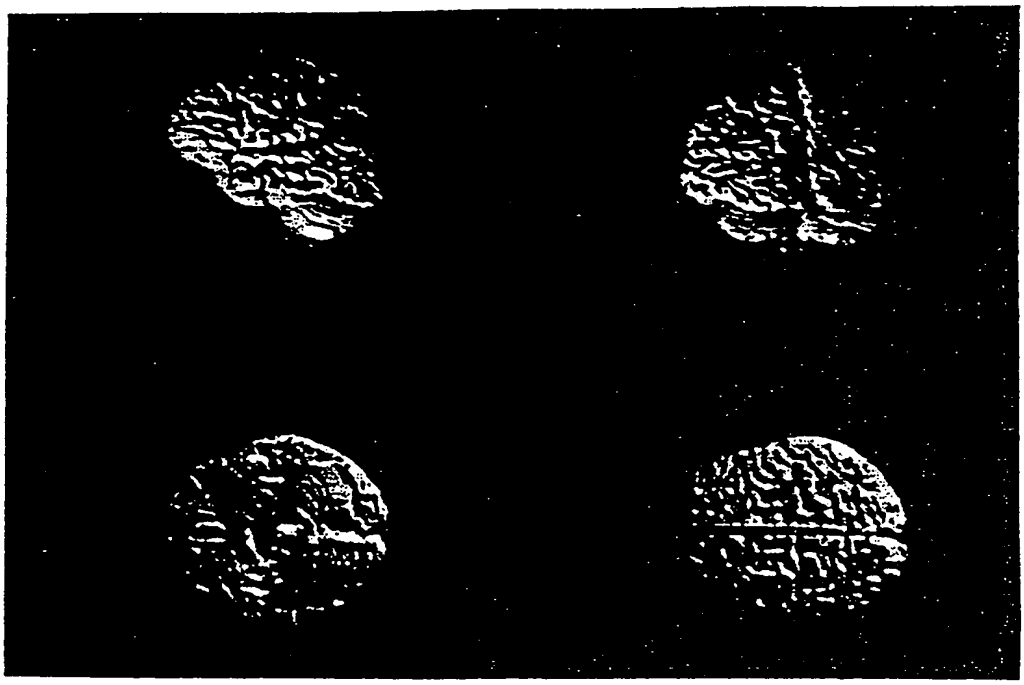

(c) (d)

Figure 12 : Sum projections (SP) of a 3–D morphologically segmented and reconstructed MRI brain scan. Brain surface is grayscale gradient enhanced and shaded with a single light source at a direction from infinity. (a) Lateral sagittal SP (b) Near posterior coronal SP (c) Inferior transverse SP (d) Superior transverse SP. The method of visualization is based on a voxel based surface enhancement [5, 21]. The classification of internal brain anatomy has also been approached with multi–modal fusion techniques [8, 11].

Analysis and Segmentation with Fuzzy Operators for Representation/Visualization

(a) (b)

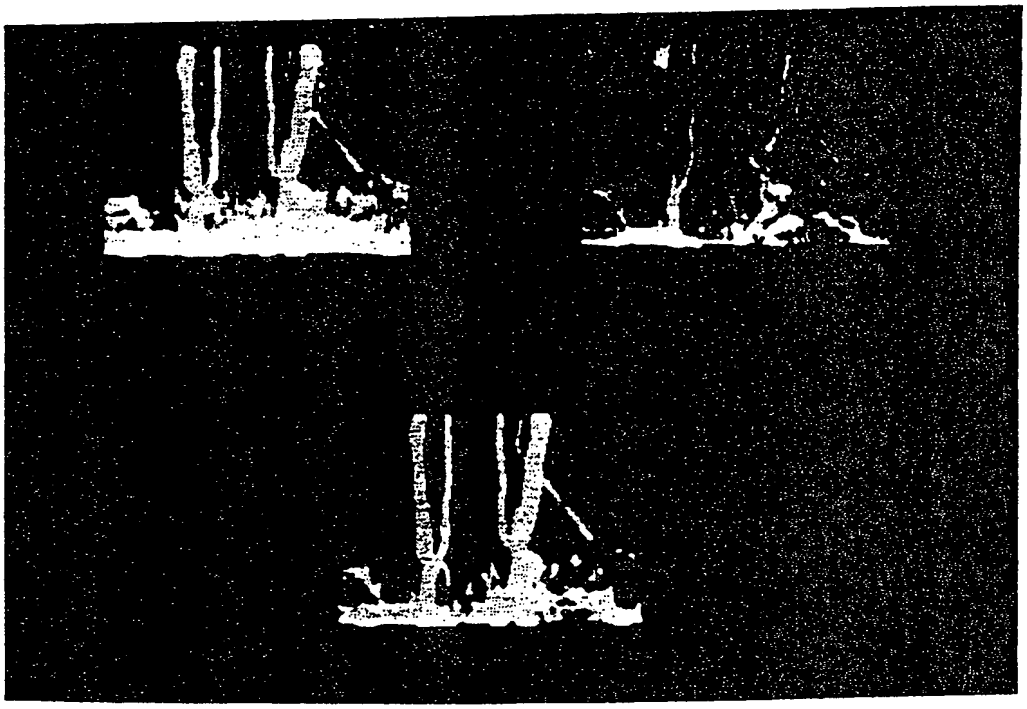

(c)

Figure 13 : Coronal sum projections (SP) of variously 3–D processed MRA acquisition of the carotid arteries, phase saturated. (a) Surface enhanced SP (b) SP of the morphological skeleton demonstrating curvilinear features, note the uniform diametric representation (c) SP of the 3–D acquisition.

Analysis and Segmentation with Fuzzy Operators for Representation/Visualization

(a) (b) (c)

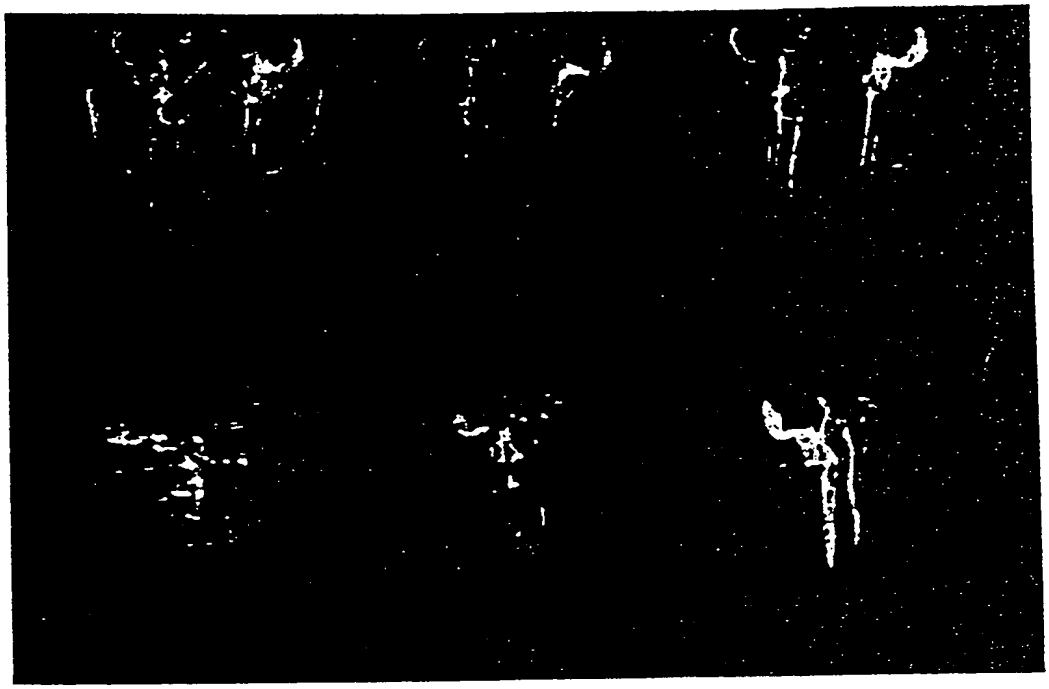

(d) (e) (f)

Figure 14 : Demonstration of variously 3–D processed MRA acquisitions with coronal sum projection (SP), top row is coronal sum projection (SP), bottom row is near lateral SP (a, d) SP of original data, posterior and anterior sections removed to reveal basal arteries, note the obscuring facial capillaries in (d). (b, e) SP of curvilinear (CV) enhanced limited morphological skeleton (LMS). (c, f) SP of morphologically reconstructed data from CVE limited morphological skeleton, note the preservation of delicate arterial features and the filtering of facial capillaries.

(a) (b) (c)

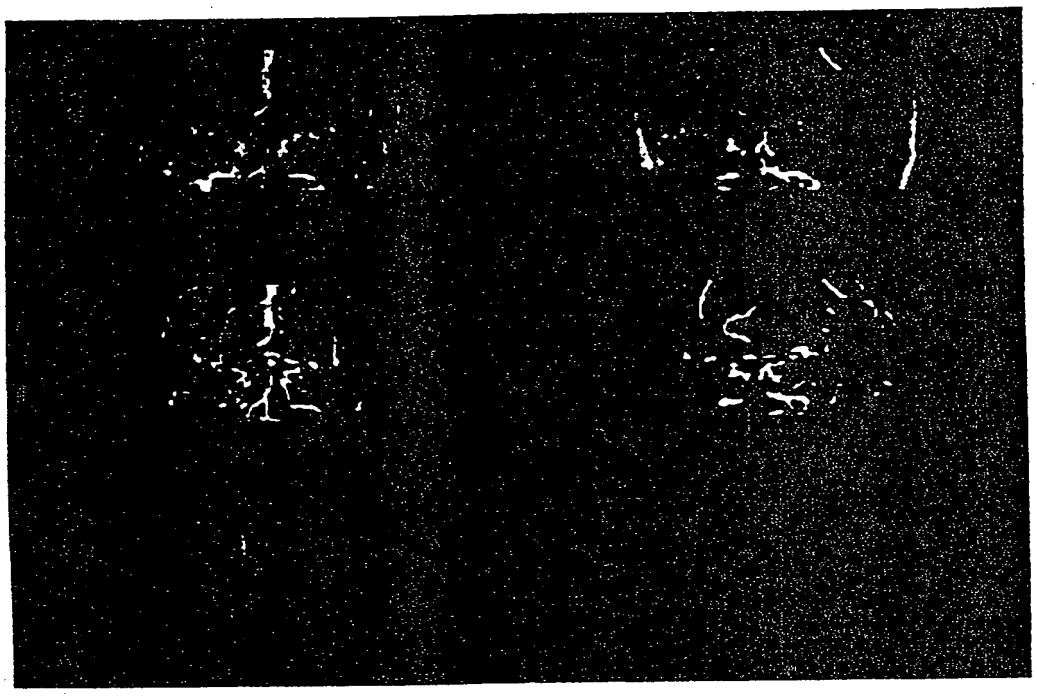

(d) (e) (f)

Figure 15 : Sum projections (SP) of blood vascular and static brain tissue features, left column is an anterior coronal SP, right row is a near left lateral SP (a, b) SP of MRA acquisition with limited scale reconstruction. (c, d) SP of CV enhancement of intracranial blood vasculature. Segmentation of intracranial vasculature was realized with segmented static brain tissues. (e, f) Fused surface shaded visualization of vasculature and static brain tissues.

(a) (b)

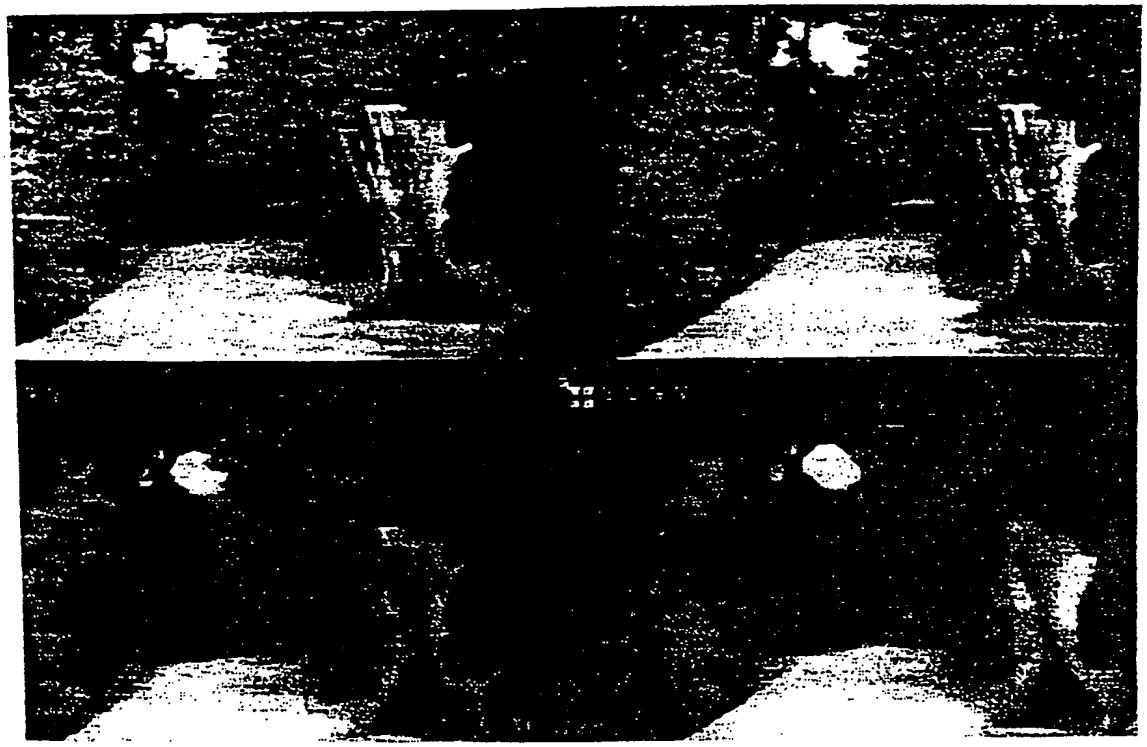

(c) (d)

Figure 16 : Median filtering on 2–D imagery provides a means of removing fractal dimesional features and "filling" textures for an alternate texture mapping. The original image (a) is decomposed into median erosion skeleton components and reconstructed with eq. (26) (b). In (c) the original image is processed with 20 cascaded operations of median erosion. In (d) the image of (c) is processed with 20 median closing operations.

(a) (b)

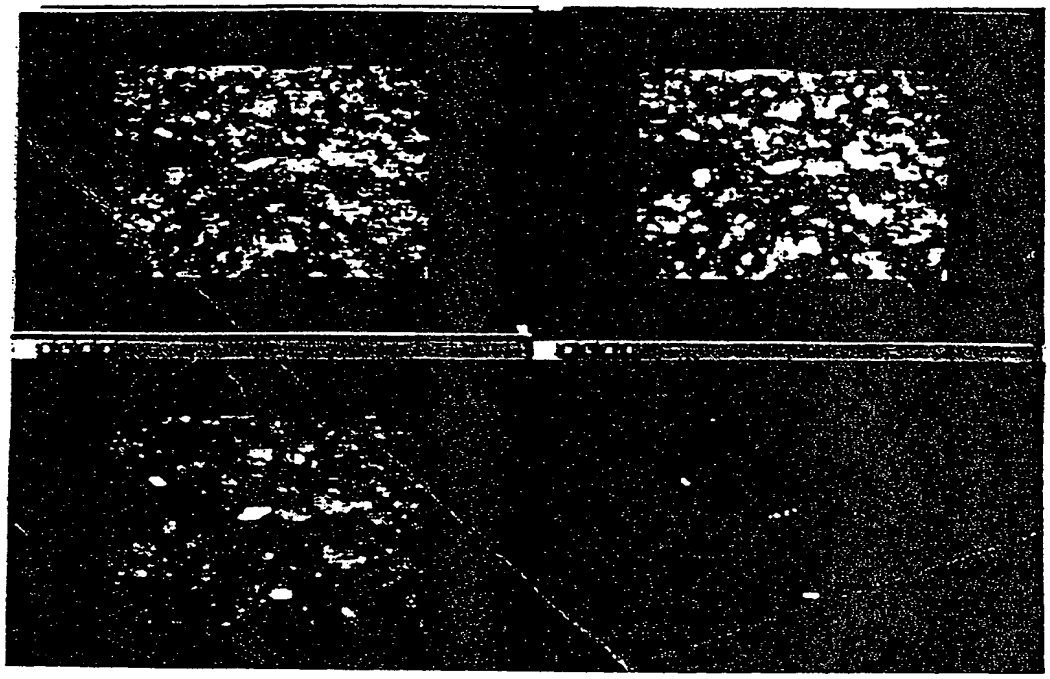

(c) (d)

Figure 17 : Median filtering on 2-D imagery provides a means of removing fractal dimesional features and "filling" textures for an alternate texture mapping. The original synthetic aperture radar (SAR) image (a) is median closed with 8 operations in (b). 32 operations in (c) 128 operations in (d).

WHAT IS CLAIMED IS:

1. A method for isolating anatomical structures contained within a three-dimensional data set, the method comprising the steps of:

a) forming a morphological skeleton of the three-dimensional data set;

b) selecting a seed data point within the morphological skeleton, the seed data point being contained within the desired anatomical structure; and

c) utilizing fuzzy connectivity to define additional data points of the desired anatomical structure so as to reconstruct substantially only the desired anatomical structure;

d) wherein reconstruction of substantially only the desired anatomical structure facilitates viewing and analysis thereof.

2. The method as recited in Claim 1 wherein the step of forming a morphological skeleton comprises recursive opening and erosion of the three-dimensional data set so as to form a plurality of residuals which define the morphological skeleton.

3. The method as recited in Claim 1 wherein the step of forming a morphological skeleton comprises utilizing a generally spherical structuring element in recursive opening and erosion of the three-dimensional data set.

4. The method as recited in Claim 1 wherein the step of selecting a seed data point comprises positioning a cursor at a desired point on an image being displayed on a monitor.

5. The method as recited in Claim 1 wherein the step of using fuzzy connectivity to define additional data points of the desired anatomical structure comprises defining connectivity based upon the size and shape of a structuring element utilizing a fuzzy generalization of mathematically defined distances between sets of data

points as a criterion.

6. The method as recited in Claim 1 wherein the step of reconstructing substantially only the desired anatomical structure comprises recursive dilation and closing of a selected portion of the morphological skeleton.

7. The method as recited in Claim 1 wherein the step of utilizing fuzzy connectivity to define additional data points comprises defining connectivity based upon the use of a generally spherical structuring element for defining distances between adjacent data points.

8. The method as recited in Claim 1 wherein the three-dimensional data set comprises a data set generated by a device selected from the group consisting of:

a) a magnetic resonance imaging device;

b) a computer aid tomography device; and

c) a positron emission tomography.

9. A method for facilitating analysis of three-dimensional medical images, the method comprising the steps of:

a) separating anatomical features from one another via dimensional filtering; and

b) storing desired separated features for analysis.

10. A method for facilitating analysis of three-dimensional medical images, the method comprising the steps of:

a) defining anatomical features having less than one dimension from the image via first dimensional filter and storing those features;

b) defining anatomical features having less than two dimensions from the image via a second dimensional filter and storing those features;

c) defining anatomical features having less than three dimensions from the image via a third dimensional filter and storing those features; and

d) storing remaining features having three dimensions in a fourth memory;

e) wherein anatomical features of different dimensionalities are thus separated from one another so as to facilitate isolation of desired anatomical structures.

11. A method for reconstructing an anatomical structure from a morphological skeleton, the method comprising:

a) selecting a seed data point within the morphological skeleton, the seed data point being contained within the desired anatomical structure; and

b) utilizing fuzzy connectivity to define additional data points of the desired anatomical structure so as to reconstruct substantially only the desired anatomical structure;

c) wherein the use of fuzzy connectivity results in reconstruction of substantially only the desired anatomical structure and substantially lacks surrounding tissue.

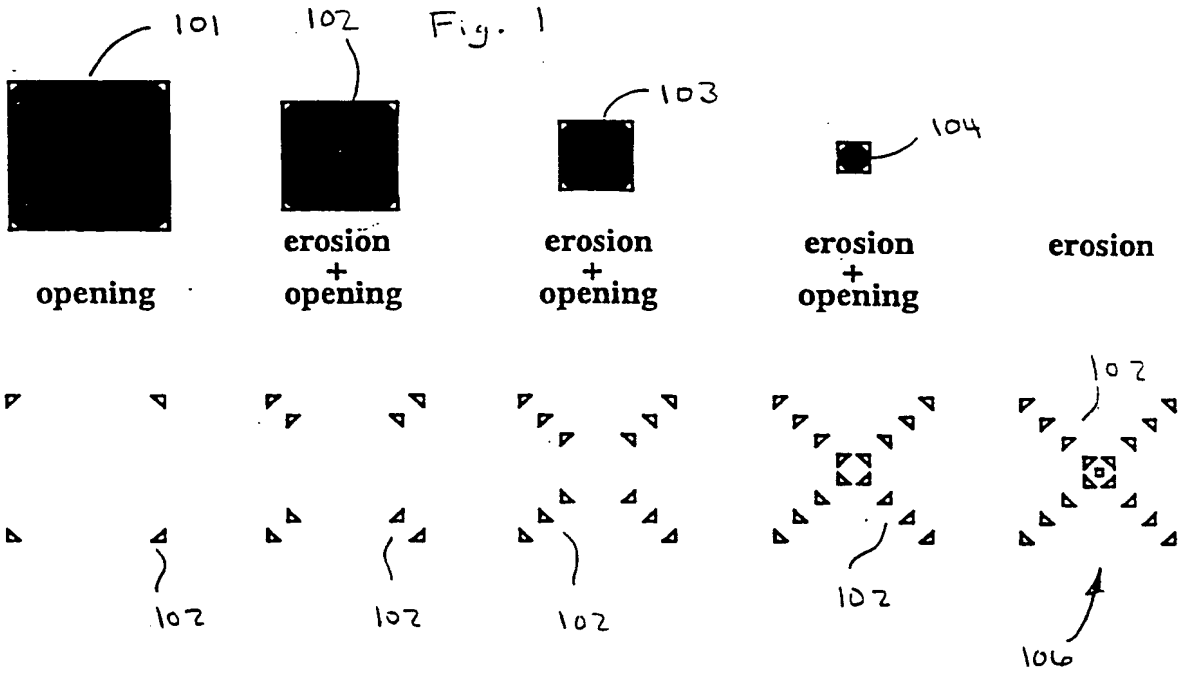

Fig. 1

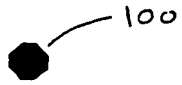

Fig. 2

structuring element form	image form: point	curve	surface	volume
point	point	curve	surface	volume
segment	null	curve	surface	volume
disk	null	null	surface	volume
sphere	null	null	null	volume

Fig. 3

Fig. 4

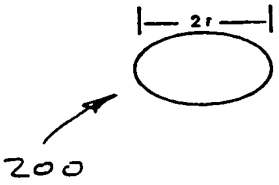

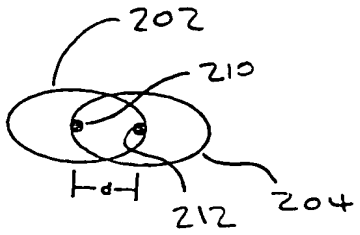

Fig. 5

Fig. 6

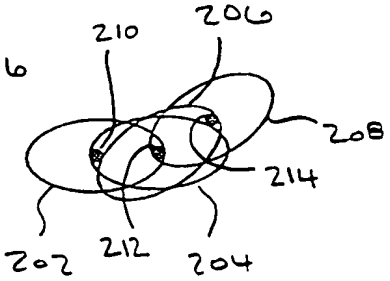

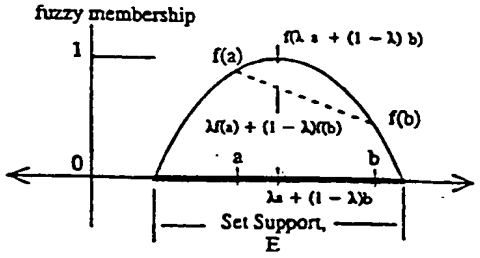

Fig. 7

Fig. 8

Standard Morphological Data Decomposition and Reconstruction

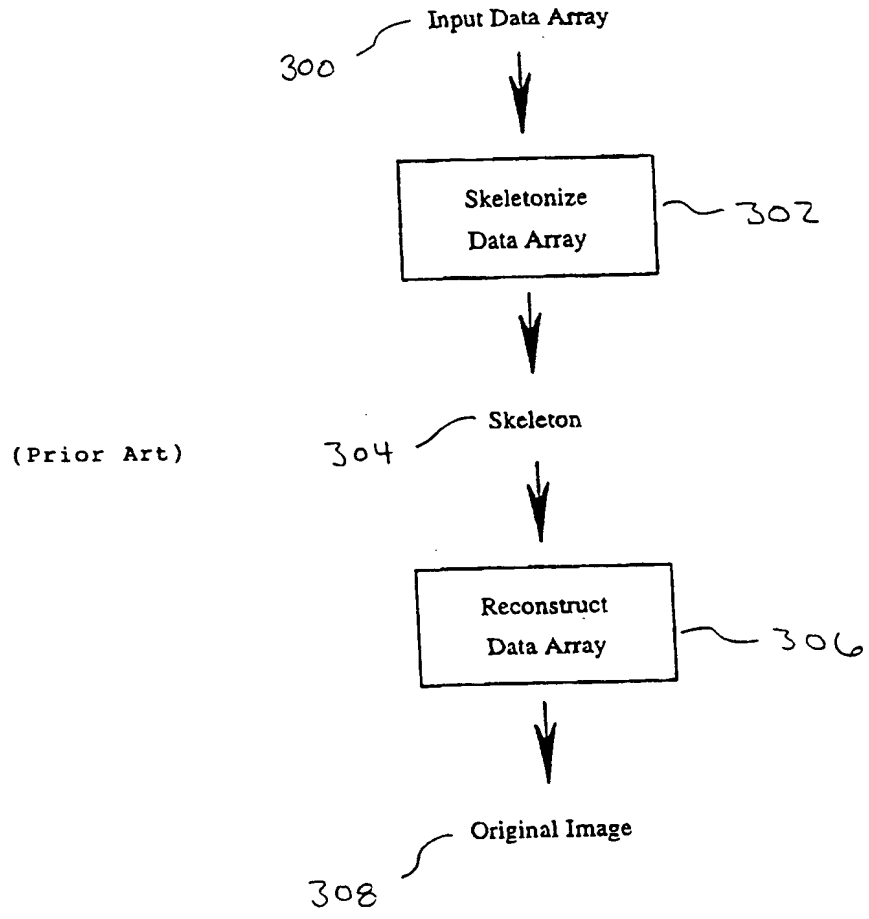

(Prior Art)

Fig. 9

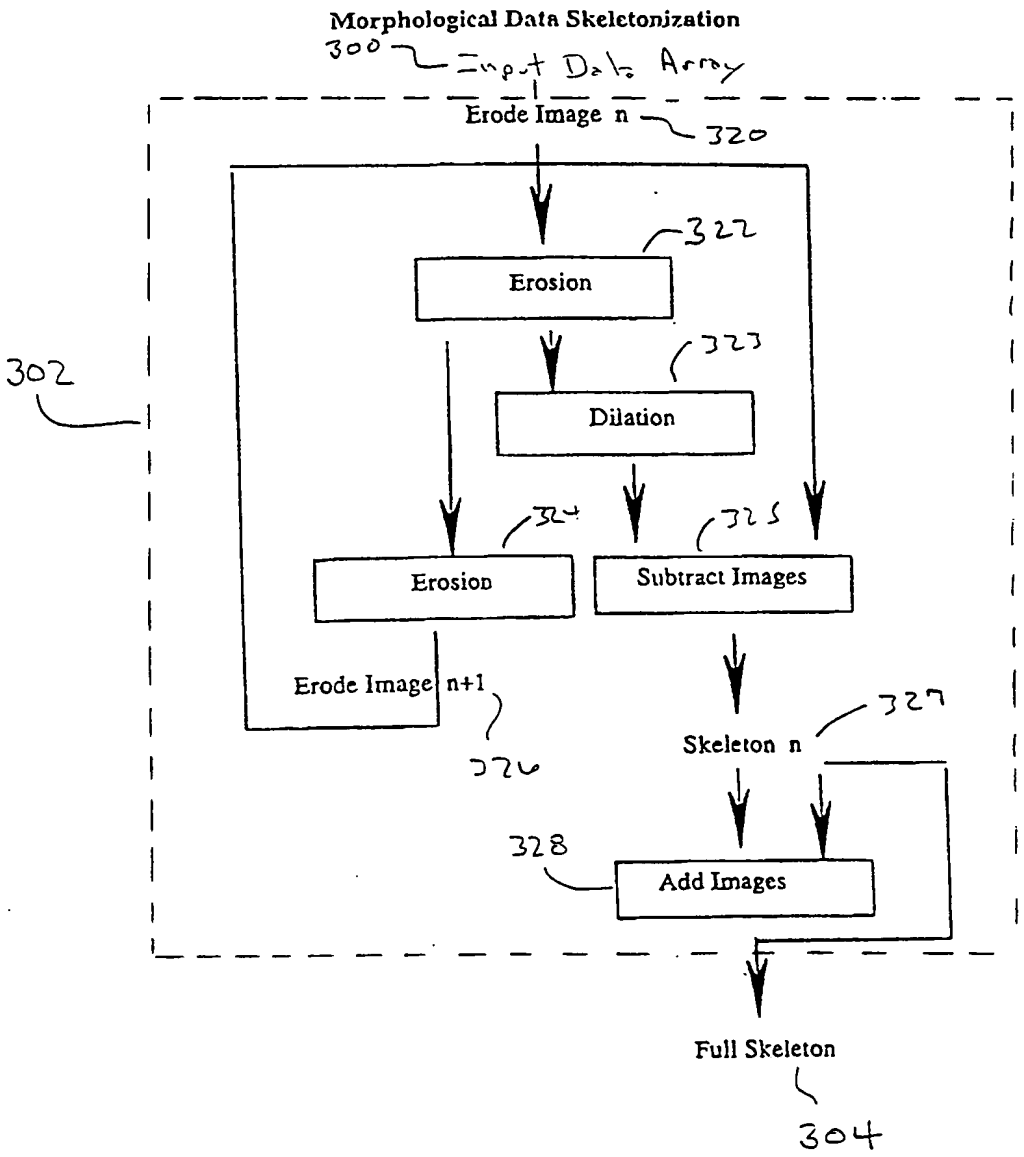
Morphological Data Skeletonization
300
Input Data Array
Erode Image n
320
322
Erosion
323
Dilation
302
324
325
Erosion
Subtract Images
Erode Image n+1
326
Skeleton n
327
328
Add Images
Full Skeleton
304

Fig. 10

Morphological Data Decomposition and Selective Reconstruction

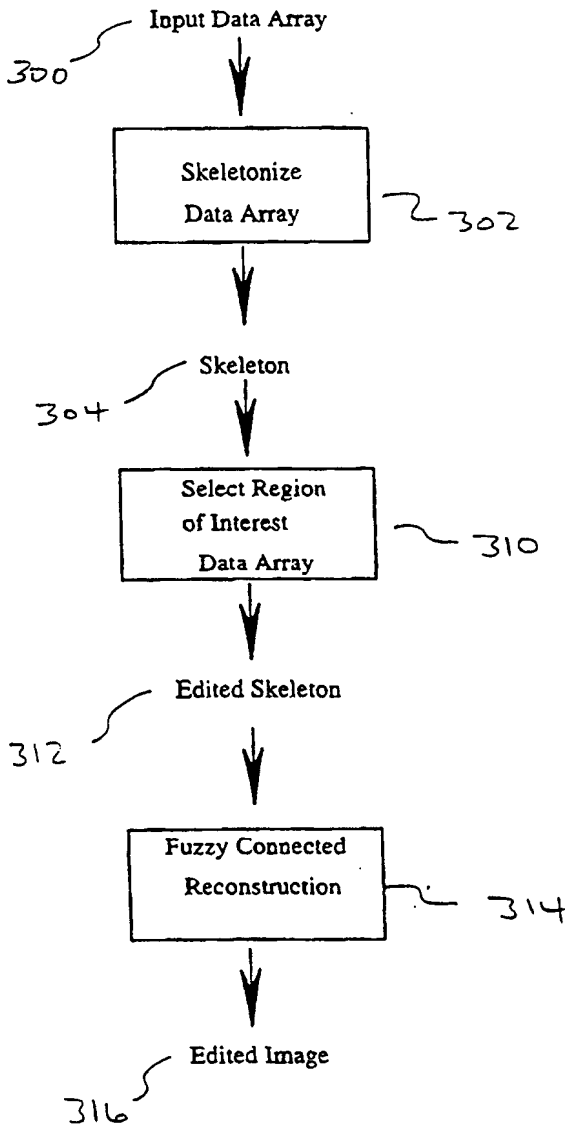

Fig. 11

Morphological Data Dimensional Sieving Decomposition and Selective Reconstruction/3D Example

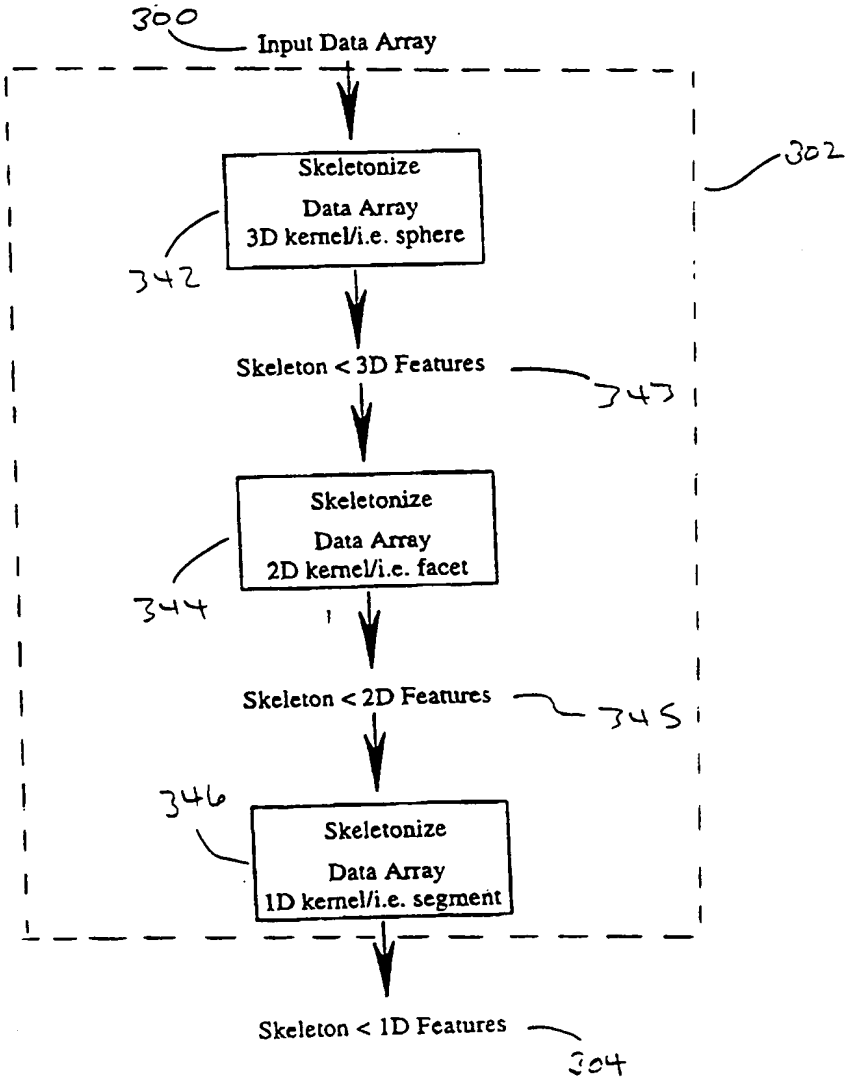

Fig. 12

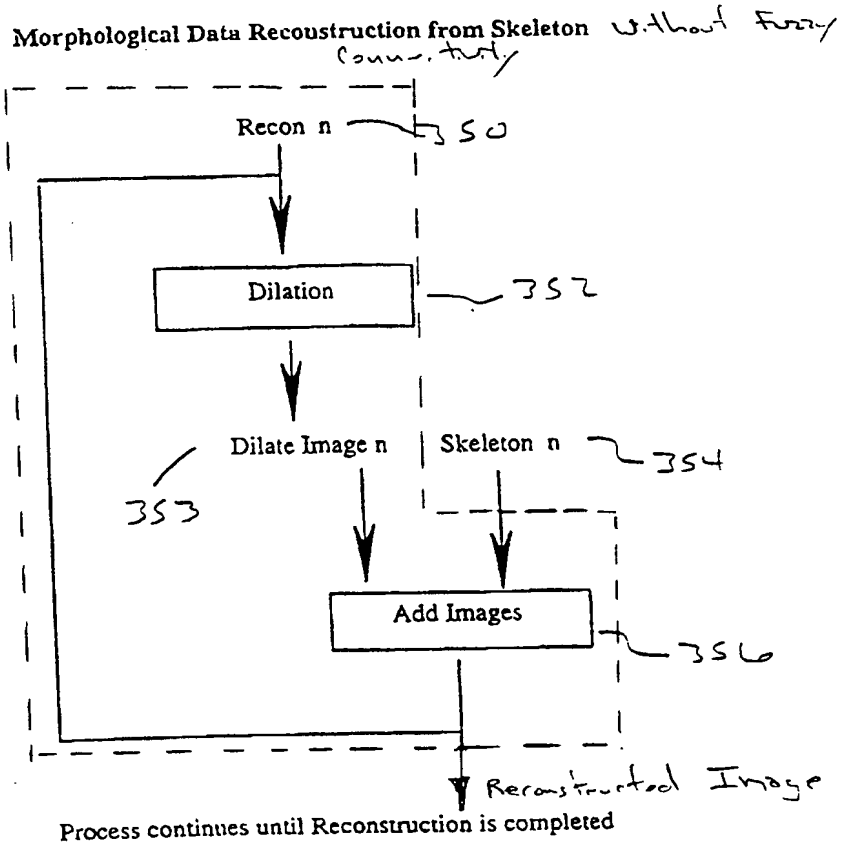
Morphological Data Recoustruction from Skeleton without Fuzzy Connectivity
Recon n
350
Dilation
352
Dilate Image n
353
Skeleton n
354
Add Images
356
Reconstructed Image
Process continues until Reconstruction is completed

Fig. 13

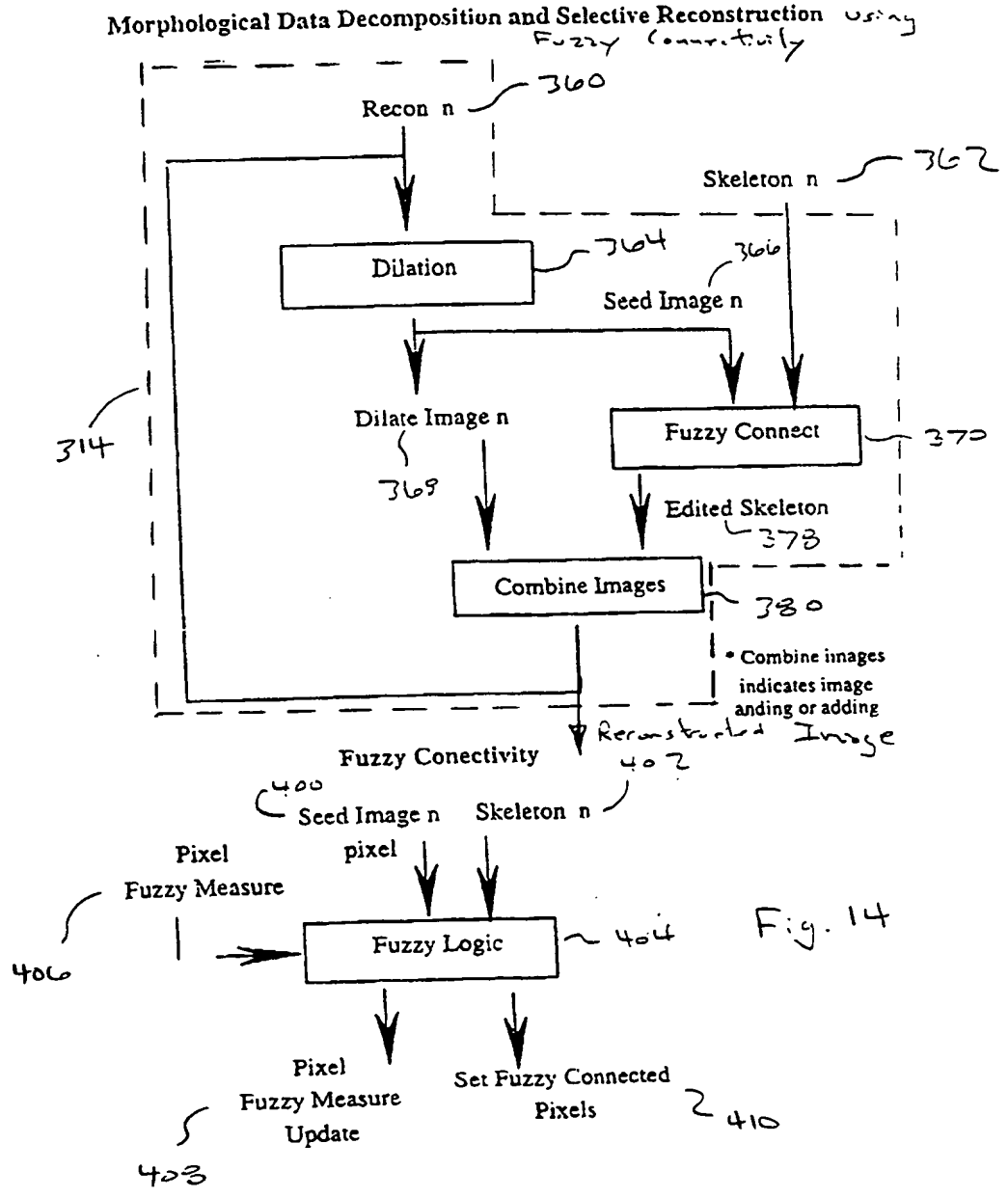
Morphological Data Decomposition and Selective Reconstruction using Fuzzy Connectivity
Recon n
360
Skeleton n
362
Dilation
364
366
Seed Image n
Dilate Image n
369
Fuzzy Connect
370
314
Edited Skeleton
378
Combine Images
380
• Combine images indicates image anding or adding
Reconstructed Image
407
Fuzzy Conectivity
400
Seed Image n
Skeleton n
Pixel
pixel
Pixel Fuzzy Measure
406
Fuzzy Logic
404
Pixel Fuzzy Measure Update
403
Set Fuzzy Connected Pixels
410

Fig. 14

INTERNATIONAL SEARCH REPORT

International application No.
PCT/US96/14500

A. CLASSIFICATION OF SUBJECT MATTER

IPC(6) :G06K 9/00, 9/40
US CL :382/128, 257, 259, 260
According to International Patent Classification (IPC) or to both national classification and IPC

B. FIELDS SEARCHED

Minimum documentation searched (classification system followed by classification symbols)

U.S. : 382/128, 257, 259, 260

Documentation searched other than minimum documentation to the extent that such documents are included in the fields searched

Electronic data base consulted during the international search (name of data base and, where practicable, search terms used)

APS, IEEE, DIALOG

C. DOCUMENTS CONSIDERED TO BE RELEVANT

Category*	Citation of document, with indication, where appropriate, of the relevant passages	Relevant to claim No.
Y	"Analysis and Segmentation of Higher Dimensional Data Sets with Fuzzy Operators for Representation and Visualization, issued 19 March 19, 1994, W. F. Kraske, pages 1-38, especially page 16, line 10 - page 17.	1-11
Y	US, A, 5,201,011 (Bloomberg et al.) 06 June 1993, col. 7, lines 37-57.	1-8, 11

☐ Further documents are listed in the continuation of Box C. ☐ See patent family annex.

*	Special categories of cited documents:	"T"	later document published after the international filing date or priority date and not in conflict with the application but cited to understand the principle or theory underlying the invention
"A"	document defining the general state of the art which is not considered to be of particular relevance	"X"	document of particular relevance; the claimed invention cannot be considered novel or cannot be considered to involve an inventive step when the document is taken alone
"E"	earlier document published on or after the international filing date	"Y"	document of particular relevance; the claimed invention cannot be considered to involve an inventive step when the document is combined with one or more other such documents, such combination being obvious to a person skilled in the art
"L"	document which may throw doubts on priority claim(s) or which is cited to establish the publication date of another citation or other special reason (as specified)	"&"	document member of the same patent family
"O"	document referring to an oral disclosure, use, exhibition or other means		
"P"	document published prior to the international filing date but later than the priority date claimed		

Date of the actual completion of the international search 13 NOVEMBER 1996	Date of mailing of the international search report 24 DEC 1996
Name and mailing address of the ISA/US Commissioner of Patents and Trademarks Box PCT Washington, D.C. 20231 Facsimile No. (703) 305-3230	Authorized officer MATTHEW C. BELLA Telephone No. (703) 305-9646

Form PCT/ISA/210 (second sheet)(July 1992)*